

RESEARCH ARTICLE

Folliculin variants linked to Birt-Hogg-Dubé syndrome are targeted for proteasomal degradation

Lene Clausen¹, Amelie Stein^{1*}, Martin Grønbæk-Thygesen¹, Lasse Nygaard¹, Cecilie L. Søltøft¹, Sofie V. Nielsen¹, Michael Lisby¹, Tommer Ravid², Kresten Lindorff-Larsen^{1*}, Rasmus Hartmann-Petersen^{1*}

1 The Linderstrøm-Lang Centre for Protein Science, Department of Biology, University of Copenhagen, Copenhagen, Denmark, **2** Department of Biological Chemistry, The Alexander Silberman Institute of Life Sciences, The Hebrew University of Jerusalem, Jerusalem, Israel

* amelie.stein@bio.ku.dk (AS); lindorff@bio.ku.dk (KL-L); rhpetersen@bio.ku.dk (RH-P)



OPEN ACCESS

Citation: Clausen L, Stein A, Grønbæk-Thygesen M, Nygaard L, Søltøft CL, Nielsen SV, et al. (2020) Folliculin variants linked to Birt-Hogg-Dubé syndrome are targeted for proteasomal degradation. *PLoS Genet* 16(11): e1009187. <https://doi.org/10.1371/journal.pgen.1009187>

Editor: Elizabeth Henske, Brigham and Women's Hospital, UNITED STATES

Received: May 6, 2020

Accepted: October 10, 2020

Published: November 2, 2020

Copyright: © 2020 Clausen et al. This is an open access article distributed under the terms of the [Creative Commons Attribution License](https://creativecommons.org/licenses/by/4.0/), which permits unrestricted use, distribution, and reproduction in any medium, provided the original author and source are credited.

Data Availability Statement: All relevant data are within the manuscript and its [Supporting Information](#) files.

Funding: Novo Nordisk Foundation challenge programme PRISM to K.L.L., A.S. & R.H.P. The Lundbeck Foundation to A.S. & L.C. The Danish Cancer Society to R.H.P. Foundation Jochum to R.H.P. Eva & Henry Frønkels Mindefond to R.H.P. The Danish Council for Independent Research (Natural Sciences) to R.H.P. & M.L. The funders had no role in study design, data collection and

Abstract

Germline mutations in the folliculin (*FLCN*) tumor suppressor gene are linked to Birt-Hogg-Dubé (BHD) syndrome, a dominantly inherited genetic disease characterized by predisposition to fibrofolliculomas, lung cysts, and renal cancer. Most BHD-linked *FLCN* variants include large deletions and splice site aberrations predicted to cause loss of function. The mechanisms by which missense variants and short in-frame deletions in *FLCN* trigger disease are unknown. Here, we present an integrated computational and experimental study that reveals that the majority of such disease-causing *FLCN* variants cause loss of function due to proteasomal degradation of the encoded FLCN protein, rather than directly ablating FLCN function. Accordingly, several different single-site FLCN variants are present at strongly reduced levels in cells. In line with our finding that FLCN variants are protein quality control targets, several are also highly insoluble and fail to associate with the FLCN-binding partners FNIP1 and FNIP2. The lack of FLCN binding leads to rapid proteasomal degradation of FNIP1 and FNIP2. Half of the tested FLCN variants are mislocalized in cells, and one variant ($\Delta E510$) forms perinuclear protein aggregates. A yeast-based stability screen revealed that the deubiquitylating enzyme Ubp15/USP7 and molecular chaperones regulate the turnover of the FLCN variants. Lowering the temperature led to a stabilization of two FLCN missense proteins, and for one (R362C), function was re-established at low temperature. In conclusion, we propose that most BHD-linked *FLCN* missense variants and small in-frame deletions operate by causing misfolding and degradation of the FLCN protein, and that stabilization and resulting restoration of function may hold therapeutic potential of certain disease-linked variants. Our computational saturation scan encompassing both missense variants and single site deletions in *FLCN* may allow classification of rare FLCN variants of uncertain clinical significance.

analysis, decision to publish, or preparation of the manuscript.

Competing interests: The authors have declared that no competing interests exist.

Author summary

Birt-Hogg-Dubé (BHD) syndrome is a dominantly inherited genetic disease characterized by predisposition to fibrofolliculomas, lung cysts, and renal cancer. The disease is linked to germline variants in the folliculin (*FLCN*) tumor suppressor gene. Here, we present a combined computational and experimental study, focusing on rare BHD-linked missense and single amino acid deletion variants. Our data show that many disease-causing *FLCN* variants lead to structural destabilization and rapid proteasomal degradation of the FLCN protein. The reduced level of FLCN, in turn, leads to degradation of the FLCN binding partners FNIP1 and FNIP2. Additional results show that the turnover of FLCN is regulated by the deubiquitylating enzyme Ubp15/USP7 and molecular chaperones. We propose that for some missense variants, stabilization and resulting restoration of function may hold therapeutic potential, and that our computational saturation scan encompassing both missense variants and single site deletions in *FLCN* may allow classification of rare FLCN variants of uncertain clinical significance.

Introduction

In order to function, most proteins require some conformational flexibility and are therefore not completely rigid in their native environment. In addition, since nature selects for function most proteins are not overly stable, and stress conditions or mutations may cause proteins to lose their native conformation and misfold. Because misfolded proteins can be toxic and form insoluble aggregates, they must be quickly eliminated from the cell via the so-called protein quality control (PQC) network [1–3]. Typically, PQC depends on molecular chaperones to associate with the misfolded proteins, and refold them or guide them for degradation via the ubiquitin-proteasome system (UPS) or autophagy [4–8]. Despite a number of recent efforts [9, 10], it is not completely understood how cells discern misfolded from native proteins but it is likely to involve recognition of exposed hydrophobic regions that are normally buried in the native protein.

Recently, we have shown for several disease-related proteins that the degree of protein destabilization correlates with the turnover rate [11–13], and a structural destabilization of as little as 3 kcal/mol is enough to trigger degradation. This is in agreement with genetic studies in yeast that have shown that the PQC system operates by following a better-safe-than-sorry principle and is thus highly diligent and prone to target proteins that are only slightly structurally perturbed but still functional [14–16]. Likewise, seminal studies in human cells have shown that some cystic fibrosis patients carry a deletion in the *CFTR* gene that result in a protein that retains biochemical function. This protein variant fails to conduct its function not because it is intrinsically inactive, but because it is targeted by the PQC system for proteasomal degradation, which in turn leads to an insufficient amount of protein and ultimately disease [17, 18]. Here, we show that a similar PQC mechanism is responsible for targeting certain variants of the folliculin protein (*FLCN*) linked to Birt-Hogg-Dubé (BHD) syndrome (OMIM: 607273) and that, similar to results for multiple other proteins, structural calculations predict these effects [11–13, 19–30].

The autosomal dominantly inherited BHD syndrome is caused by variants in the *FLCN* gene [31–33]. BHD syndrome predisposes patients to develop hair follicle hamartomas (fibrofolliculomas), lung cysts, and renal neoplasia with an age-dependent and variable penetrance [34–37]. A locus for BHD syndrome was mapped to chromosome 17p11.2 by linkage analysis in BHD families, and subsequently germline mutations in the *FLCN* gene were identified [31,

38, 39]. Further analysis of tumors from patients with BHD syndrome revealed somatic *FLCN* second hit inactivating mutations in the wild-type allele [40, 41], in line with *FLCN* having a tumor suppressor function. The tumor suppressor activity of *FLCN* is also supported by data from BHD animal models [42–44].

The widely expressed *FLCN* gene encodes the 64 kDa cytosolic and nuclear *FLCN* protein, which does not display high sequence similarity to any other human protein but is highly conserved across species [33]. Functional studies have linked *FLCN* to diverse metabolic pathways and cellular processes [33], including the mTOR signalling pathway [45], regulation of PGC1 α and mitochondrial biogenesis [46], TFE3/TFEB transcriptional regulation [47, 48], RhoA activation, cell adhesion [49], and amino acid-dependent activation of mTORC1 through Rag GTPases [50, 51]. Intriguingly, recent data have shown that wild-type *FLCN* is a HSP90 target protein and FNIP1/2 act as co-chaperones to facilitate *FLCN* folding [52, 53], thus directly linking *FLCN* to PQC.

A high-resolution crystal structure of the C-terminal domain of *FLCN* has been solved [54] and shows a remarkable structural similarity to the DENN domain in the DENN1B protein [55]. The DENN domain proteins have been found to function as guanine exchange factors (GEFs) for Rab-type GTPases and thus activate the vesicle transport function of these small GTPases [56]. Recently, a full-length structure of *FLCN* was obtained by cryo-EM [57, 58], showing that the N-terminal region of *FLCN* contains a Longin domain which forms contacts with the Longin domain in its binding partner folliculin-interacting protein (FNIP1), while the C-terminal DENN domain interacts with the DENNc domain in FNIP1. In turn, FNIP1 mediates interaction to RagA, RagC and Ragulator to control mTORC activation [57].

In addition to FNIP1, *FLCN* also associates with the related protein FNIP2 and the AMP-activated protein kinase AMPK [59–61], which in cells serves as an energy sensor and regulator of the mTOR signalling pathway. The FNIP1 and FNIP2 proteins display sequence similarity (49% identity) and similar expression patterns [60], suggesting that they may overlap in function. The link between *FLCN* function and the FNIP1/2 proteins is also supported by genetic data. Thus, mice inactivated in both *Fnip1* and *Fnip2* develop cystic kidneys similar to the phenotype observed in kidney-targeted *Fln* knock-out mice [45, 62, 63].

The vast majority of BHD-linked *FLCN* mutations are frameshift variants leading to truncations and splice site aberrations predicted to cause loss of function [33]. Truncated variants of the *FLCN* protein are likely to be structurally destabilized, engage with chaperones and eventually be degraded by the proteasome, as recently shown for the L460QsX25 variant [64]. On the other hand, the consequences of the more rare BHD-linked *FLCN* missense variants and short in-frame deletions are not well characterized, although some are likely to destabilize the *FLCN* protein [65].

Here, we show that disease-causing *FLCN* missense mutations, rather than directly ablating *FLCN* protein function, instead render the *FLCN* proteins to become PQC targets. Rapid proteasomal degradation of the *FLCN* variants results in strongly reduced steady-state *FLCN* levels in cells. Several of the variants are also insoluble and fail to associate with the *FLCN* binding partners FNIP1 and FNIP2. This lack of *FLCN* binding in turn triggers proteasomal degradation of FNIP1 and FNIP2. Some of the *FLCN* variants are mislocalized in cells and one variant (Δ E510) forms perinuclear protein aggregates. The USP7 deubiquitylating enzyme (DUB) regulates *FLCN* turnover. In agreement with the disease-linked *FLCN* variants being structurally destabilized, lowering of the temperature leads to a stabilization of the missense proteins, and for one variant function was re-established at low temperature. In conclusion, we propose that BHD-linked missense mutations operate by causing misfolding and degradation of the *FLCN* protein, and structural stabilization of certain disease-linked variants may hold therapeutic potential.

Results

Disease-associated FLCN variants display reduced steady-state levels due to proteasomal degradation

Previous studies indicate that BHD-linked FLCN missense protein variants are destabilized [65], which, in turn, suggest that they might be subject to PQC-dependent clearance. To test this hypothesis, we first analyzed the steady-state level of wild-type FLCN and eight different FLCN variants that have been found in BHD patients (Table 1). The proteins were produced untagged from the pIRES2-GFP expression vector in transiently transfected U2OS cells. In agreement with the previous report [65], we found that several of the FLCN variants were present at strongly reduced steady-state levels (Fig 1A and 1B). The reduction in the FLCN protein levels was not caused by changes in transfection efficiency or in transcription, since the level of GFP, produced from the internal ribosomal entry site (IRES) in the same mRNA as FLCN, was unchanged (Fig 1A). The most severe reduction in steady-state level was observed for the Δ E510 FLCN variant, while the levels of the V400I and K508R variants were hardly affected, compared to the wild-type FLCN control (Fig 1A and 1B). Indeed, although both V400I and K508R have been found in BHD patients, these relatively conservative substitutions occurred together with other putative pathogenic variants and their link to the disease is unclear (Table 1).

To test directly if the reduced protein levels were caused by degradation, we followed the turnover of the FLCN variants in cultures treated with the translation inhibitor cycloheximide (CHX). The wild type, V400I and K508R variants were stable, while the other variants were degraded (Fig 1C). By densitometry of Western blots, we estimate the half-life of wild-type FLCN to be $\gg 8$ hours, while the short-lived variants displayed half-lives between 3 and 8 hours (Fig 1D).

Most intracellular proteins are degraded via the proteasome or via the autophagy system. To analyze whether the observed FLCN turnover was caused by proteasomal degradation or via autophagy, we analyzed the level of the FLCN variants in cultures treated with the proteasome inhibitor bortezomib (BZ) or chloroquine (CQ), which inhibits autophagy. In case of wild-type FLCN and the stable variants, V400I and K508R, there was no effect of BZ (Fig 1E), since these variants are not rapidly degraded. Similar to overexpressed wild type FLCN, endogenous FLCN in the U2OS cells also appears stable (S1 Fig). However, for all other variants the levels were increased in response to proteasome inhibition (Fig 1E), suggesting that these variants are proteasome targets. We did not observe stabilization in the presence of CQ for any of the variants (S2 Fig).

Table 1. Stability, localization and function of FLCN variants.

FLCN variant	Protein level (%)	Half-life (hours)	Subcellular localization	Solubility	Stabilizes FNIP1/2	Binds to FNIP1/2	Stabilized at 29°C	ClinVar category	Rosetta $\Delta\Delta G$ (kcal/mol)
WT	100	>8	Cyt & Nuc	Normal	Yes	Yes	-	Benign	0
Δ F157	~33	~3	Cyt	Reduced	No	Poorly	No	Pathogenic	-
R239C	~27	~3	Cyt & Nuc	Very low	No	Yes	Yes	Conflicting	-
H255P	~29	~3	Cyt	Reduced	No	Poorly	Partially	VUS	-
R362C	~59	~8	Cyt & Nuc	Reduced	Partially	Yes	Yes	VUS	2.9
V400I	~80	>8	Cyt & Nuc	Normal	Yes	Yes	-	Conflicting	0.7
Δ K508	~31	~4	Cyt	Very low	No	Poorly	No	Pathogenic	5.0
K508R	~99	>8	Cyt & Nuc	Normal	Yes	Yes	-	Like. benign	0.02
Δ E510	~23	~6	Aggregates	Very low	No	Poorly	No	Pathogenic	4.0

<https://doi.org/10.1371/journal.pgen.1009187.t001>

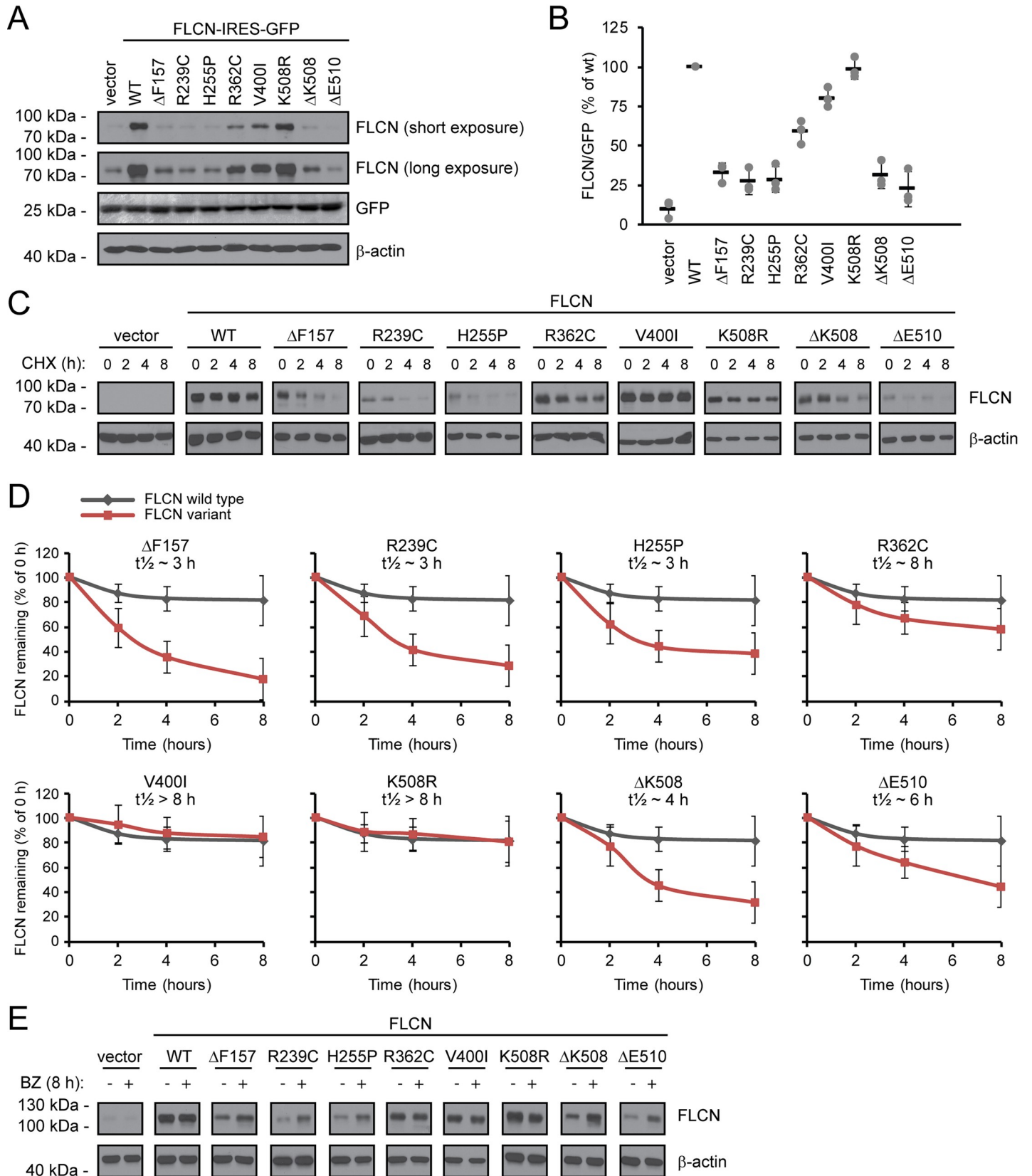


Fig 1. BHD-linked FLCN variants are rapidly degraded by the proteasome. (A) The protein levels of wild-type (WT) FLCN and the FLCN variants in U2OS whole cell lysates determined by SDS-PAGE and Western blotting with antibodies to FLCN. GFP and β -actin served as controls for equal transfection efficiency and loading, respectively. Endogenous FLCN was only visible upon longer exposures. (B) Quantification of blots as shown in (A) by densitometry normalized to the GFP level. The level of wild-type FLCN was set to 100%. The error bars show the standard deviation ($n = 3$). (C) The degradation of the FLCN variants was followed in cultures treated with the translation inhibitor cycloheximide (CHX) by SDS-PAGE and Western blotting of whole cell lysates with antibodies to FLCN. β -actin served as a loading control. (D) Quantification of blots as shown in (C) by densitometry normalized to the level at 0 hours. The error bars show the standard deviation. ($n = 3$). (E) The steady-state levels in whole cell lysates of the FLCN variants were compared in cultures incubated with or without the proteasome inhibitor, bortezomib (BZ), for 8 hours. β -actin served as a loading control.

<https://doi.org/10.1371/journal.pgen.1009187.g001>

***In silico* analyses suggest that pathogenic FLCN variants are structurally destabilized**

We performed biophysical calculations to estimate the effects of the different FLCN variants on protein stability ($\Delta\Delta G$). The $\Delta\Delta G$ values quantify the loss or gain of favourable or destabilizing molecular interactions in the protein conformation induced by the missense variant or deletion, with high $\Delta\Delta G$ values indicating greater destabilization and thus more likely recognition by the PQC system. The calculations are structure-based and were only carried out for the C-terminal domain of FLCN, for which high-resolution structural details are available (residues 341 to 566, PDB 3V42, see also Fig 2A) [54].

For missense variants, it is well-established that many have neutral or slightly destabilizing effects, and only a fraction of the possible single amino acid changes are severely detrimental [66–68]. In contrast, there is far less data on protein stability for in-frame deletions, though existing studies on certain model proteins show that a number of both insertions and deletions are functional [69–72]. All three deletions in our initial dataset, however, are severely destabilized (Fig 1). Thus, we aimed to identify putative non-deleterious deletion variants and validate those experimentally.

We calculated $\Delta\Delta G$ s for missense variants with Rosetta [12, 73, 74] (Fig 2B and 2C). For in-frame deletions, we modified a previously described protocol [75]. Briefly, this consists of creating the sequence of the deletion variant of interest, creating a homology model using the original crystal structure (PDB: 3V42) as the template, relaxing this model with Rosetta, and calculating the energy difference ($\Delta\Delta G$) to the original structure (see Methods). This approach models both the effect of losing the side chain and backbone, but also the strain on the overall structure from the deletion (Fig 2D). All data are included in the supplemental material (S1 Dataset). Data for the selected variants are included in Table 1.

Similar to previous studies [11–13, 66, 76] we observe good correlation between predicted $\Delta\Delta G$ s and experimentally determined protein levels. Notably, both missense variants and in-frame deletions can be well-tolerated but can also lead to substantial loss of stability and degradation (Fig 2B). In addition to the disease-associated variants in our dataset, we tested several additional deletion and missense variants. These additional variants (Fig 2E), have, as far as we know, not been observed in patients or in population sequencing studies [77] and were only included here to test the *in silico* stability predictions. They include two predicted and experimentally confirmed stable in-frame deletions $\Delta E455$ and $\Delta A474$ (Fig 2E). In contrast, K508A shows substantially reduced stability, confirming the importance of the Lys side chain at position 508 (Fig 2D). The $\Delta E509$ variant was predicted to be as detrimental as its neighbours $\Delta K508$ and $\Delta E510$, however, it is only moderately destabilized (Fig 2E). We speculate that this may be because the side chain points into solvent, where it is less critical than in the core of the folded protein, although this is not perfectly captured by our computational model. Lastly, we compared the predicted $\Delta\Delta G$ s with the variant allele frequency as reported in gnomAD [77]. Similar to previously analysed proteins [11–13] this shows a “fishtail” distribution where the more common variants such as V400I and K508R have near-neutral stability changes, while some of the rarest and pathogenic variants are destabilized (Fig 2F).

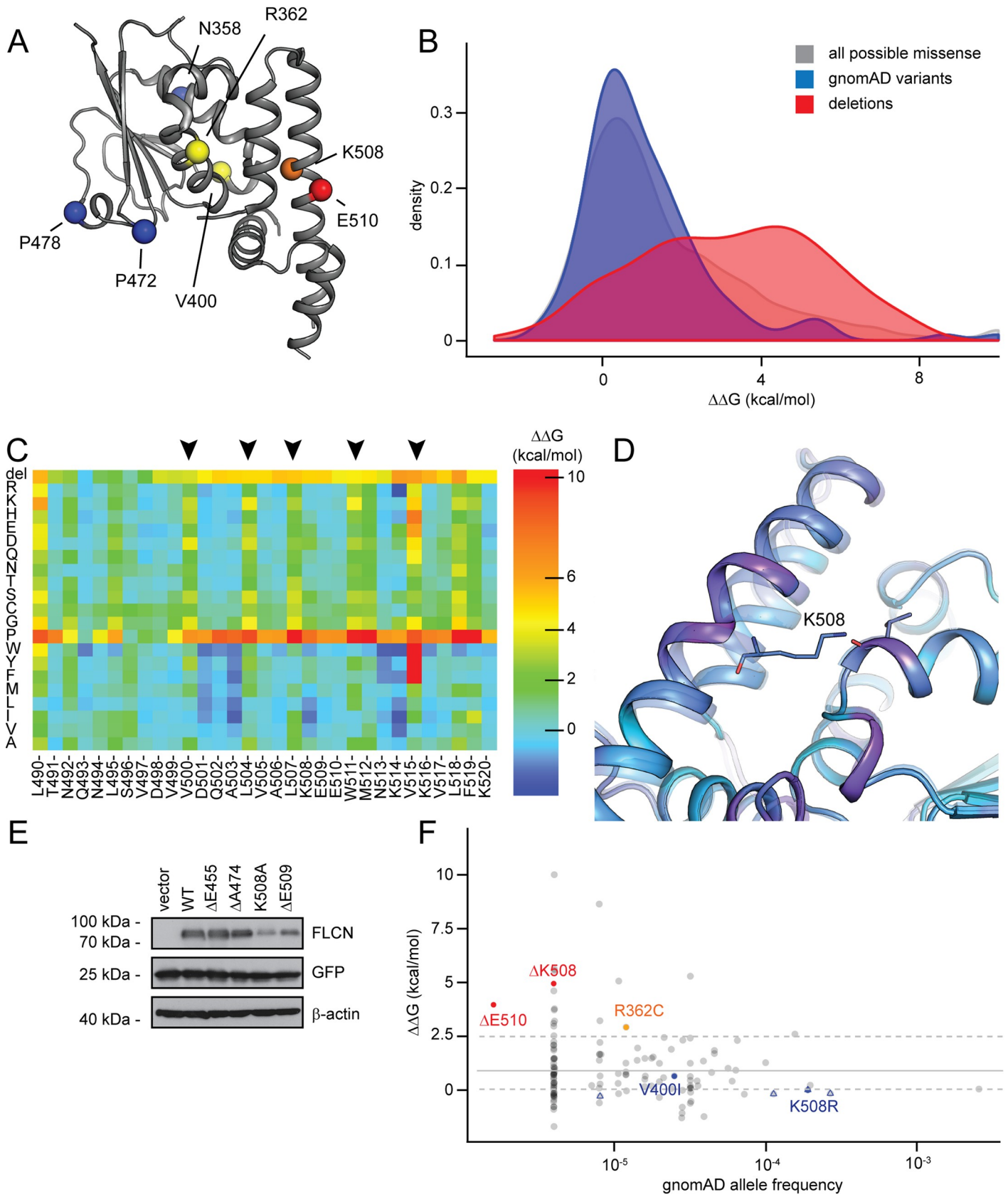


Fig 2. Structural consequences of the FLCN in-frame deletions. (A) Overview of the C-terminal domain of the FLCN crystal structure (PDB: 3V42) used for the structural calculations. Positions experimentally assayed in this work are indicated with spheres (red, deletions; yellow, missense variants; orange, position K508 with both missense variant and in-frame deletion; blue, benign ClinVar entries). (B) Distribution of $\Delta\Delta G$ s for all possible individual missense variants (gray), the subset of missense variants observed in gnomAD, and all possible individual deletions (red) in the C-terminal domain. For calculation details see [Methods](#). (C) Heat map for the segment from position 490–520 visualizing both missense and deletion (del, top row) $\Delta\Delta G$ s. A large part of this sequence forms an alpha helix, and positions that point into the domain core (arrowheads) are more constrained than those pointing towards the solvent. (D) Structural model for the deletion of K508. Deletion model in solid tracing, wild-type transparent. The helix is strained (magenta) and the hydrogen bond which K508 forms with the backbone of T393 is lost. (E) The steady-state levels of the indicated FLCN variants in whole cell lysates were compared by blotting. β -actin served as a loading control. These additional variants were tested based on stability calculations. K508A leads to loss of hydrophobic interaction and the side-chain-backbone hydrogen bond described in (D) and is thus predicted to be less stable. $\Delta E445$ and $\Delta A474$ are in linker regions and predicted to not substantially destabilize the structure. $\Delta E509$ was predicted to be as destabilizing as its neighbors $\Delta K508$ and $\Delta E510$, however, experimentally it is only mildly destabilized. This may be because its side chain points into solvent, whereas the side chains of K508 and E510 make important contacts with other parts of the C-terminal domain of FLCN. (F) “Fishtail plot” illustrating the gnomAD allele frequency of missense and deletion variants vs. the Rosetta $\Delta\Delta G$. Empty blue triangles represent benign ClinVar entries. Common and benign variants have near-neutral effects on stability, while several pathogenic variants are predicted to lose stability.

<https://doi.org/10.1371/journal.pgen.1009187.g002>

Several FLCN variants are insoluble and mislocalized

Supported by the thermodynamic predictions, the reduced steady-state levels and increased proteasomal turnover suggest that the FLCN variants are misfolded and become PQC targets. In some cases, protein misfolding results in the formation of insoluble aggregates [76, 78, 79]. To test this for the FLCN variants, we separated crude cell lysates into soluble (supernatant) and insoluble (pellet) fractions by centrifugation and analyzed the abundance of the FLCN variants in these fractions by Western blotting. Wild-type FLCN was found both in the soluble fraction and, presumably by interaction with membranes, in the pellet (S3 Fig). Several of the FLCN variants, particularly the R239C, $\Delta K508$ and $\Delta E510$ variants, were mostly insoluble (S3 Fig), suggesting that they are misfolded and may form aggregates.

Next, we proceeded to directly assess the subcellular localization of the FLCN variants by fluorescence microscopy. Consistent with other reports [45, 60, 61], wild-type FLCN was evenly distributed throughout the cytosol and nucleus (Fig 3A). This was also the case for the R239C, R362C, V400I and K508R variants. However, the nuclear localization of the other FLCN variants was strongly reduced, and in case of the $\Delta E510$ variant, most of the cells (~70%) displayed several perinuclear aggregate-like structures (Fig 3A). Accordingly, retention of the $\Delta E510$ variant was also apparent in filter trap assays (Fig 3B and 3C), where aggregated proteins fail to migrate through a nitrocellulose membrane [80].

The absence of nuclear-localized FLCN has been observed for an unstable FLCN splice variant before [81], and considering the unstable nature of these proteins, this could suggest that the observed increased protein turnover is restricted to the pool of nuclear FLCN. However, repeating the localization experiments in the presence of bortezomib did not result in any increased nuclear localization of the unstable variants or did otherwise affect the subcellular distribution of the FLCN variants (S4 Fig). This indicates that the lack of nuclear signal is caused primarily by a failure in nuclear import of FLCN rather than increased specific degradation of nuclear FLCN.

FLCN binding protects FNIP1 and FNIP2 from proteasomal degradation

Genetic and structural studies have shown that FLCN function is intimately linked to its binding partners FNIP1 and FNIP2 [33, 57], and we therefore investigated the interplay between the FLCN variants and FNIP1/2. Upon introducing HA-tagged FNIP1 or FNIP2 expression constructs, we observed very low FNIP1/2 levels (Fig 4A and 4B). Since the FNIP1/2 levels increased in response to the proteasome inhibitor bortezomib (S5 Fig), the low steady-state levels of FNIP1/2 are caused by proteasomal degradation (Fig 4A and 4B, S5 Fig). However, upon co-expression of wild-type FLCN, the FNIP1/2 proteins were dramatically stabilized (Fig 4A and 4B), suggesting that FLCN protects FNIP1/2 from degradation. Indeed, when

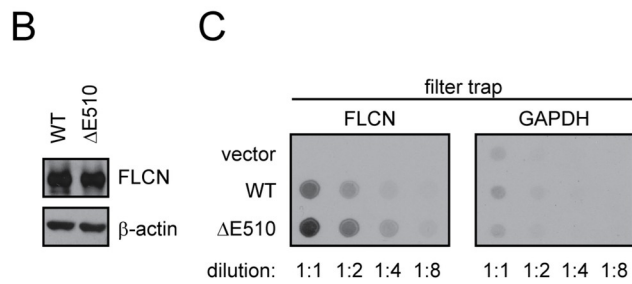
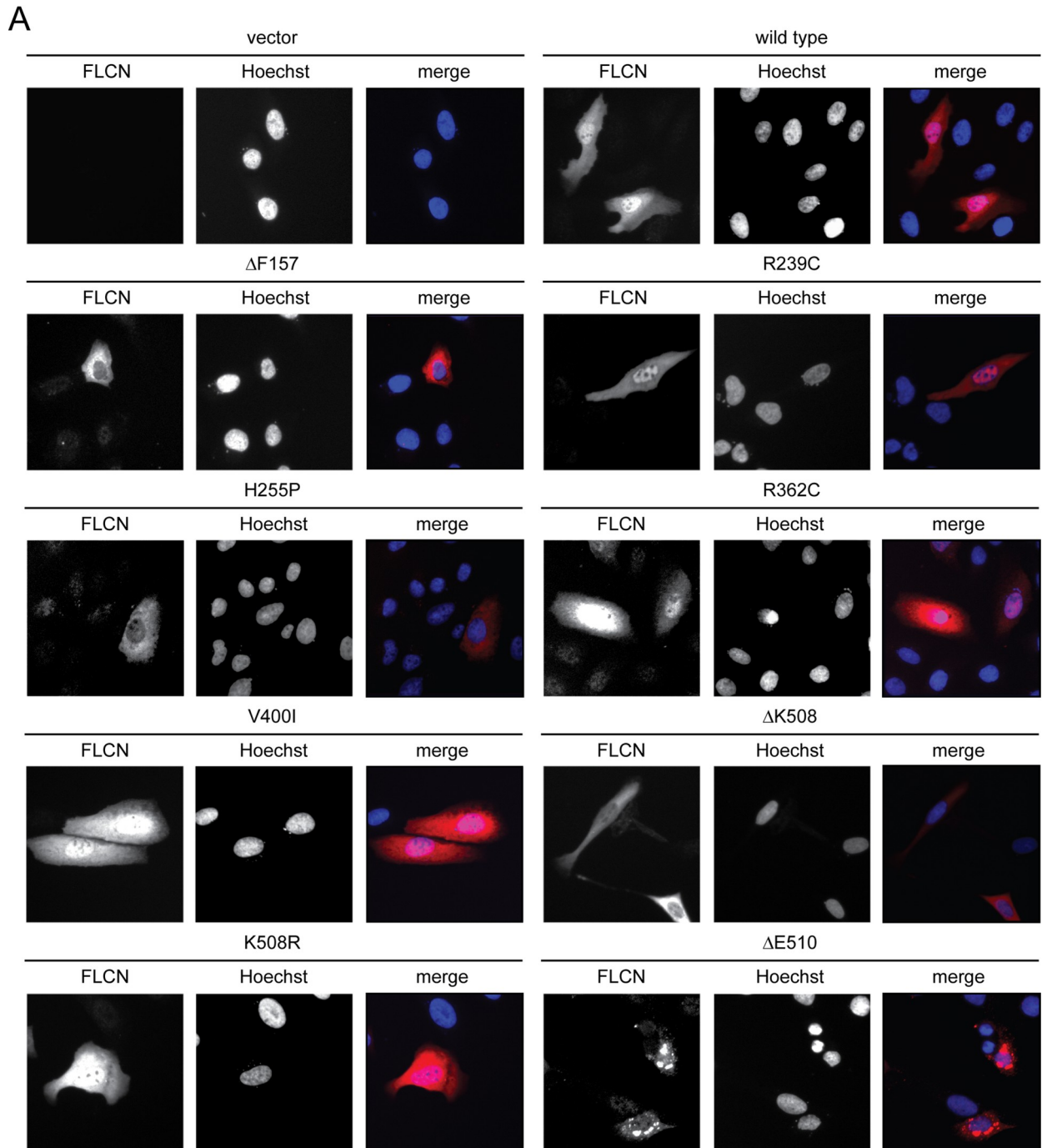


Fig 3. Certain BHD-linked FLCN variants are mislocalized. (A) The localization of the FLCN variants in transiently transfected U2OS cells was determined using antibodies to the 6His-tag. Hoechst was used to stain the nucleus. (B) As shown by SDS-PAGE and Western blotting of whole cell lysates, equal steady-state levels of wild-type (WT) FLCN and the $\Delta E510$ variant were achieved by diluting the amount of WT FLCN plasmid with empty vector prior to transfection. (C) Dilution series of the whole cell lysates shown in (B) were filtered on a nitrocellulose membrane with a pore size of 0.2 μm and developed as a Western blot using antibodies to FLCN and, as a control, to GAPDH.

<https://doi.org/10.1371/journal.pgen.1009187.g003>

following the amount of FNIP1 and FNIP2 in cycloheximide-treated cultures (Fig 4C and 4D), the FNIP1/2 proteins were rapidly degraded ($t_{1/2} \sim 16$ hours), but stabilized ($t_{1/2} \gg 16$ hours) by co-expression of FLCN (Fig 4C, 4D, 4E and 4F). Co-expression of the stable BHD-linked FLCN variants V400I and K508R, and to a lesser extent R239C and R362C, also led to FNIP1/2 stabilization, while this was less apparent for the unstable FLCN variants (Fig 4G and 4H). In agreement with earlier observations [52, 59, 60], we also observed a stabilizing effect of FNIP2 on FLCN (e.g. $\Delta F157$) (Fig 4H), indicating that FLCN and FNIP1/2 mutually stabilize each other upon complex formation.

As a further test, we also analyzed the FLCN disease-linked frameshift variant H429Pfs. This variant is missing the C-terminal part of FLCN, including a region involved in FNIP binding (S6 Fig). Accordingly, this variant is also not able to stabilize FNIP1/2 and displays strongly reduced binding to FNIP1/2 (S6 Fig).

Based on these data, we reasoned that FNIP1 and FNIP2 are protected from proteasomal degradation upon FLCN binding. Accordingly, in co-precipitation experiments with FNIP1/2 the V400I, K508R, R239C, and R362C FLCN variants all appeared adept at FLCN interaction, while the FNIP1/2 binding was strongly reduced for the other FLCN variants (Fig 5A and 5B). Co-expression of FNIP1 and FNIP2 did not lead to any mutual stabilization (Fig 5C), excluding that FNIP stabilization by FLCN occurs indirectly e.g. via a FNIP1-FNIP2 interaction.

A yeast screen links FLCN turnover to chaperones and the deubiquitylating enzyme Ubp15/USP7

To further analyze the degradation of the unstable FLCN variants we took advantage of a yeast selection system for protein stability [9]. Specifically, we expressed wild-type FLCN (as a control) and the unstable $\Delta E510$ variant as fusion proteins with the orotidine-5'-phosphate (OMP) decarboxylase Ura3 enzyme in a strain carrying a deletion of the endogenous *URA3* gene (*ura3 Δ*) (Fig 6A). Since proteasomal protein degradation is processive [82], degradation of the $\Delta E510$ fusion protein should lead to reduced amounts of the Ura3 fusion partner. Accordingly, we observed the FLCN $\Delta E510$ fusion protein was rapidly degraded via the proteasome (Fig 6B), and the $\Delta E510$ strain displayed a reduced growth in media lacking uracil (Fig 6C). As expected the growth defect was completely suppressed by addition of sublethal amounts of the proteasome inhibitor bortezomib (Fig 6C), and we therefore continued to screen for components targeting the unstable FLCN variants for degradation. To this end, the $\Delta E510$ yeast expression construct was introduced into a library of 4992 individual gene deletion mutants [83], one-by-one, by mating. After sporulation and selection of haploid cells with the gene deletion (G418 resistant) and the Ura3 reporter fusion construct, the resulting haploids were scored for growth by monitoring the colony sizes on solid media lacking uracil. In total 27 mutants caused significantly increased growth, suggesting a stabilization of the $\Delta E510$ variant, while 135 mutants displayed a significantly reduced growth, indicating that the $\Delta E510$ variant was less abundant in these cells. All 162 significant hits from this screen are included in the supplemental material (S2 Dataset). To test the validity of the screen we selected two hits, *ydj1 Δ* and *ubp15 Δ* , for further analyses. In agreement with the results from the high-throughput screen, introducing the $\Delta E510$ fusion in *ydj1 Δ* cells led to a visibly increased growth, while

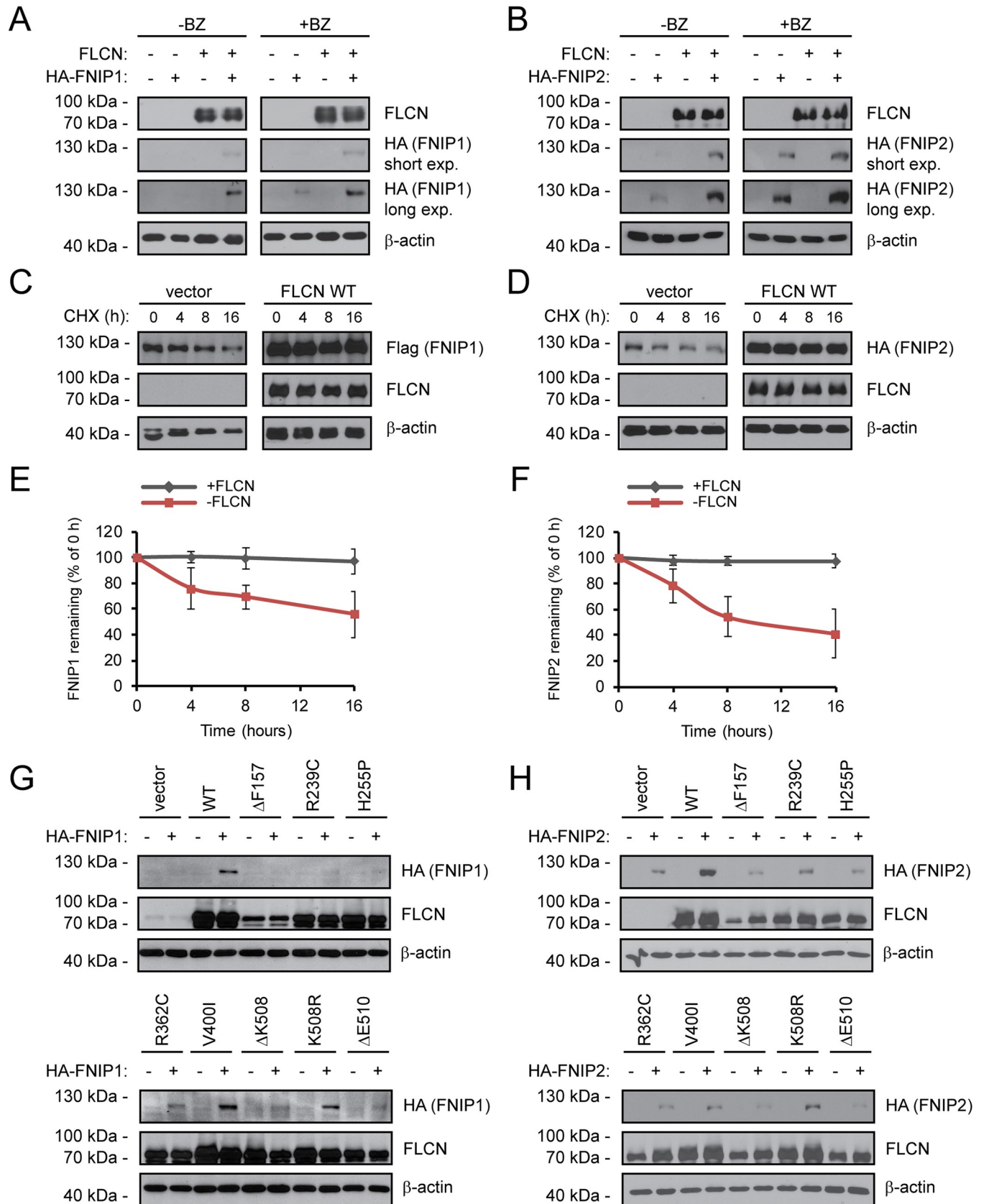


Fig 4. FLCN stabilizes FNIP1 and FNIP2. (A) U2OS cells transiently transfected to express either FLCN, HA-tagged FNIP1, or both FLCN and HA-FNIP1, were either untreated or treated with the proteasome inhibitor bortezomib (BZ) for 8 hours. Then the levels of FLCN and FNIP1 in whole cell lysates were compared by SDS-PAGE and Western blotting with antibodies to FLCN or the HA-tag on FNIP1. β -actin served as a loading control. (B) U2OS cells transiently transfected to express either FLCN, HA-tagged FNIP2, or both FLCN and HA-FNIP2, were either untreated or treated with the bortezomib. Then the levels of FLCN and FNIP2 in whole cell lysates were compared by SDS-PAGE and Western blotting with antibodies to FLCN or the HA-tag on FNIP2. β -actin served as a loading control. (C) The degradation of FNIP1 in the presence or absence of co-transfected FLCN was followed in cultures treated with the translation inhibitor cycloheximide (CHX) by SDS-PAGE and Western blotting of whole cell lysates with antibodies to the Flag-tag on FNIP1. FLCN and β -actin served as controls. (D) The degradation of FNIP2 in the presence or absence of co-transfected FLCN was followed in cultures treated with the translation inhibitor cycloheximide (CHX). (E) Quantification of blots as shown in (C) by densitometry normalized to the level at 0 hours. The error bars show the standard deviation ($n = 3$). (F) Quantification of blots as shown in (D) by densitometry normalized to the level at 0 hours. The error bars show the standard deviation ($n = 3$). (G) The levels of FLCN and FNIP1 were compared by SDS-PAGE and Western blotting in whole cell lysates of U2OS cells transiently transfected to express HA-tagged FNIP1 and the indicated FLCN variants. FLCN was detected with antibodies to FLCN. FNIP1 was detected using antibodies to the HA-tag. (H) The levels of FLCN and FNIP2 were compared by SDS-PAGE and Western blotting in whole cell lysates of U2OS cells transiently transfected to express HA-tagged FNIP2 and the indicated FLCN variants. FLCN was detected using antibodies to FLCN. FNIP2 was detected using antibodies to the HA-tag. In all panels β -actin served as a loading control.

<https://doi.org/10.1371/journal.pgen.1009187.g004>

the *ubp15 Δ* cells appeared to grow more poorly (Fig 6D). This difference was also apparent in the steady-state levels of the Δ E510 fusion. Hence, in *ydj1 Δ* cells we observed a higher level of Δ E510 fusion protein, while in the *ubp15 Δ* strain, the Δ E510 protein level was reduced (Fig 6E).

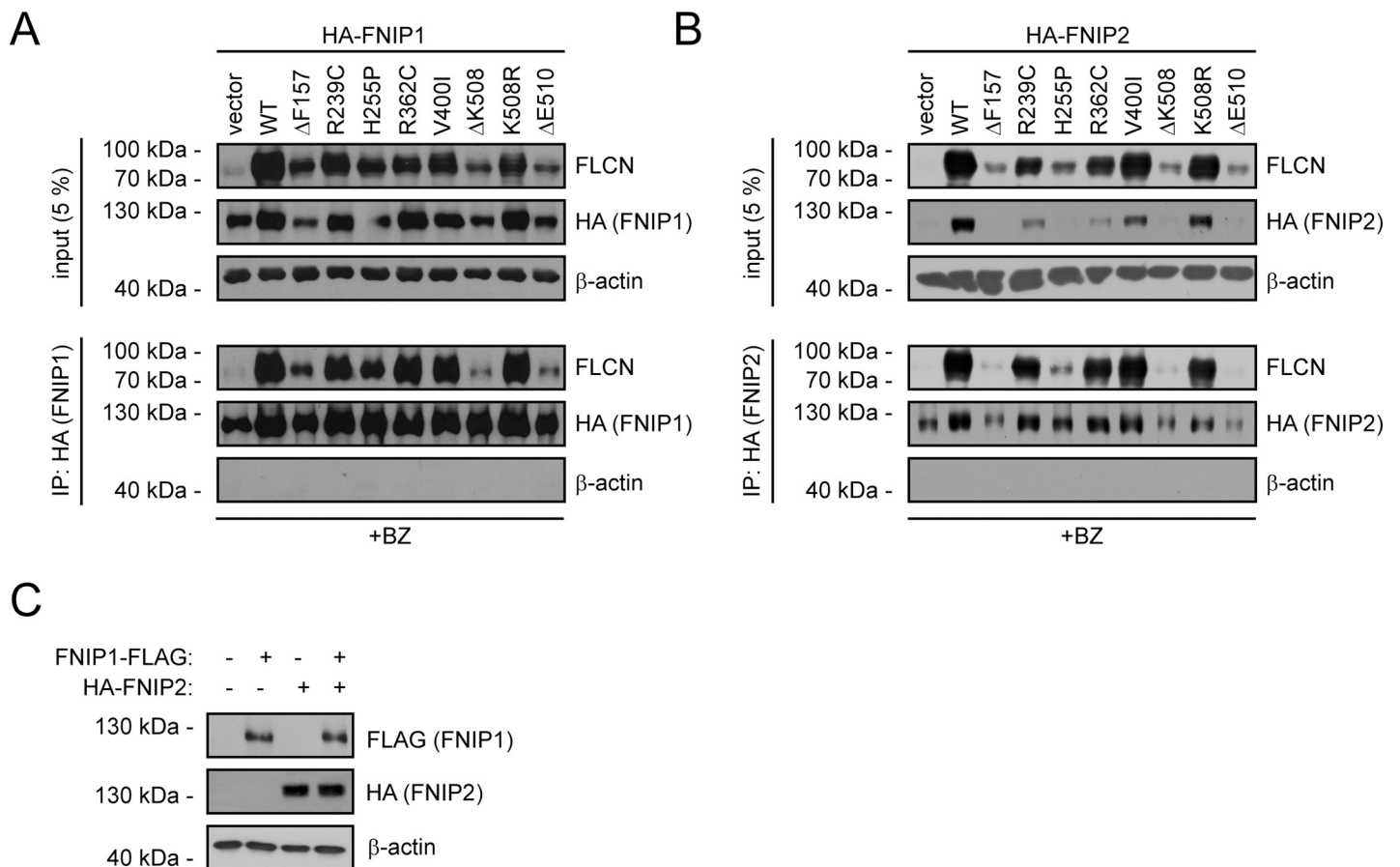


Fig 5. Some FLCN variants display reduced FNIP1/2 binding. (A) The FLCN variants were analyzed for interaction with FNIP1. HA-tagged FNIP1 was immunoprecipitated and analyzed by blotting. Input samples (5%) were included as a control. To obtain an adequate amount of the FNIP1 and FLCN proteins, the cells were treated with bortezomib, for 8 hours before harvest. (B) The FLCN variants were analyzed for interaction with FNIP2. HA-tagged FNIP2 was immunoprecipitated and analyzed by blotting. Input samples (5%) were included as a control. Similar to above, the cells were treated for 8 hours with bortezomib (BZ) prior to harvesting and lysis. (C) Whole cell lysates of U2OS cells, transiently transfected to express either Flag-tagged FNIP1, HA-tagged FNIP2, or both, were analyzed by blotting.

<https://doi.org/10.1371/journal.pgen.1009187.g005>

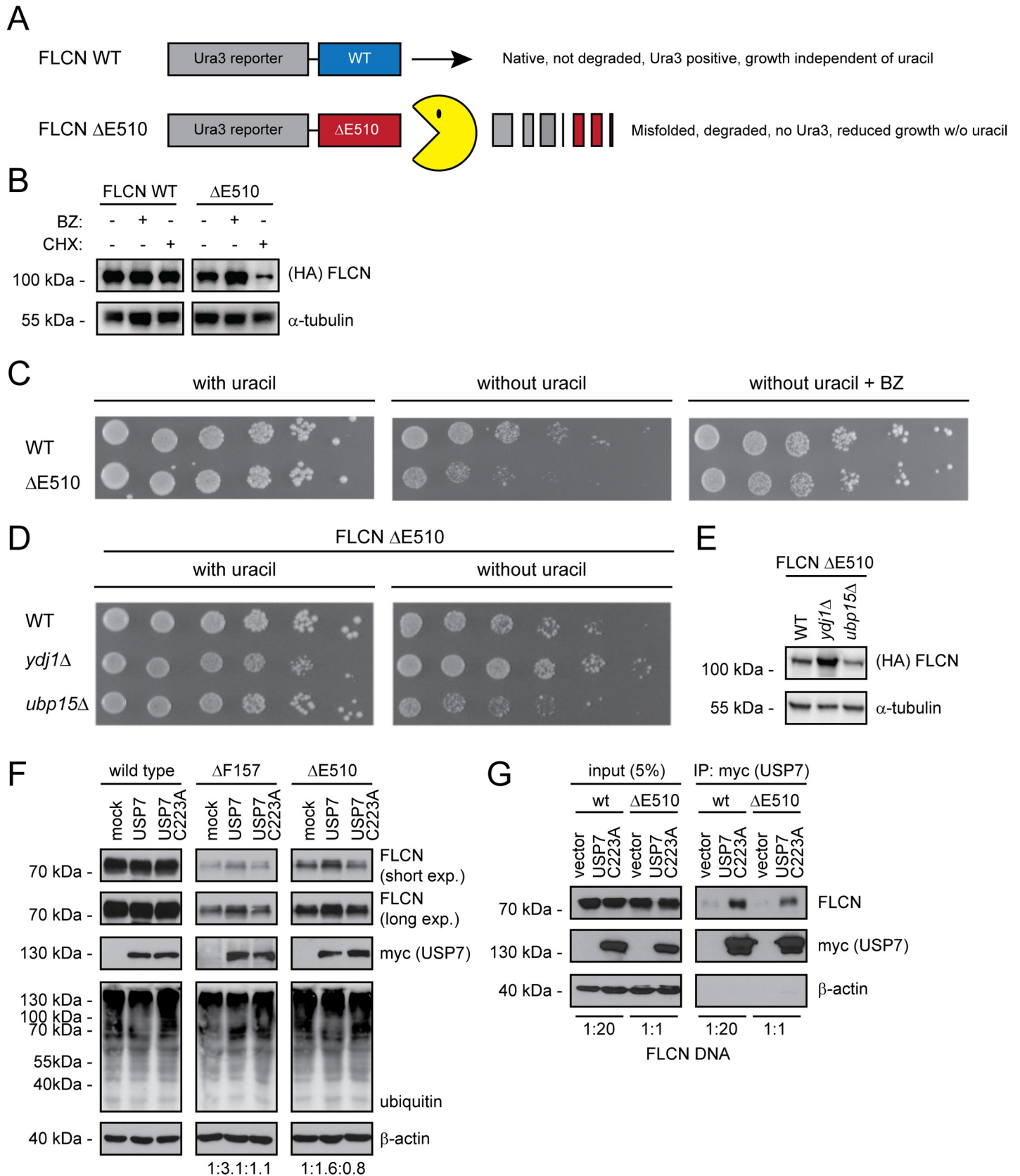


Fig 6. The USP7 DUB regulates FLCN protein levels. (A) Schematic illustration of the utilized yeast system for high-throughput scoring of FLCN protein stability. Briefly, either wild-type FLCN or the $\Delta E510$ FLCN variant is fused to the C-terminus of a HA-tagged Ura3-reporter protein. In case of the $\Delta E510$ FLCN variant, we expect the protein to be destabilized and degraded (Pac-Man), leading to reduced levels of the Ura3 protein and thereby a decreased growth in the absence of uracil. (B) The amount of FLCN and FLCN $\Delta E510$ Ura3-fusion protein was analyzed in whole cell lysates of cultures treated with (+) or without (-) 1 mM of the proteasome inhibitor bortezomib (BZ) for 3 hours, or where protein synthesis was inhibited with 100 $\mu\text{g}/\text{ml}$ of cycloheximide (CHX) for 4 hours. For detection on Western blots antibodies to HA (to detect FLCN), and, as a loading control, to α -tubulin, were used. (C) Growth of wild-type yeast cells transformed with Ura3-fusion vectors for wild-type (wt) FLCN or FLCN $\Delta E510$ was compared by spotting serial dilutions on solid media with uracil (left panel), without uracil (central panel), or without uracil, but supplemented with bortezomib (BZ) (right panel). (D) Growth wild-type (WT), *ydj1* Δ and *ubp15* Δ yeast cells transformed with the Ura3-fusion vector for FLCN $\Delta E510$ was compared by spotting serial dilutions on solid media with uracil (left panel) and without uracil (right panel). (E) The level of the FLCN $\Delta E510$ Ura3-fusion protein in whole cell lysates was compared by blotting using antibodies to HA (to detect FLCN), and, as a loading control, to α -tubulin. (F) FLCN variants were transfected into U2OS cells with an expression vector for either wild-type myc-tagged USP7 or the catalytically dead USP7 C223A variant. Whole cell lysates were analyzed by SDS-PAGE and Western blotting using antibodies to FLCN, myc (to detect the co-expressed USP7) and ubiquitin. β -actin served as a loading control. Quantification of the FLCN (short exposure) signals in fold compared to mock transfected is given below. (G) The wild-type and $\Delta E510$ FLCN variants were analyzed for interaction with the catalytically dead USP7 C223A variant. Myc-tagged USP7 was immunoprecipitated using the myc-trap system and analyzed by blotting. Input samples (5%) were included as a control. To achieve equal amounts of the FLCN proteins, the cells were transfected with 20-fold less wild-type FLCN DNA compared to FLCN $\Delta E510$ DNA.

<https://doi.org/10.1371/journal.pgen.1009187.g006>

Ydj1 is a DnaJ domain family co-chaperone linked to proteasomal degradation of misfolded chaperone clients [10], while Ubp15 is a deubiquitylating enzyme which counteracts E3s to block degradation. Whereas human cells encode a number of J-domain proteins that are homologous to the yeast Ydj1, the yeast Ubp15 is in human cells represented by a single orthologue called USP7. Next, we therefore co-transfected U2OS cells to express FLCN and either wild-type USP7 or, as a control, a catalytically dead USP7 variant carrying a C223A substitution of the active site cysteine residue. We note that the overexpression of USP7 did not affect the overall ubiquitylation of cell proteins (Fig 6F), suggesting that USP7 is specific for a subset of ubiquitylated proteins. In agreement with the results in yeast cells, overexpression of the wild-type USP7, but not of the catalytically dead USP7 variant, led to a slight stabilization of the FLCN $\Delta F157$ and $\Delta E510$ variants (Fig 6F), suggesting that USP7 deubiquitylates these proteins to subtly regulate their cellular abundance. However, in case of the frameshift FLCN H429Pfs we did not observe any effect of USP7 (S6 Fig).

Since we found that FLCN contains multiple potential TRAF- and UBL1/2-domain binding consensus motifs (S7 Fig, S8 Fig) that could mediate direct interaction to USP7 [84], we tested if FLCN and USP7 interact by co-precipitation. To achieve equal amounts of wild type and $\Delta E510$, we transfected the U2OS cells with 20-fold less plasmid encoding wild-type FLCN compared to $\Delta E510$, but equal amounts of a plasmid encoding myc-tagged USP7 C223A. We observed a clear interaction between USP7 and FLCN (Fig 6G), supporting further a role of USP7 in regulating FLCN turnover. Since USP7 is also associated with wild-type FLCN, it is possible that it also plays a regulatory role in FLCN function.

Effect of temperature on FLCN stability and function

In some cases, PQC targets can be stabilized structurally by lowering the temperature, which in turn leads to a reduced degradation and increased steady-state level [11]. To test this for the FLCN variants, we compared their steady-state levels at 37°C and 29°C. Importantly, lowering the temperature to 29°C does not affect the ubiquitin-proteasome system in U2OS cells (S9 Fig) [11]. Several of the FLCN variants were stabilized at 29°C (Fig 7A), indicating that these variants are indeed structurally stabilized at the lower temperature. This effect was most apparent for the R362C variant (Fig 7A), in line with our observation that this variant is borderline stable already at 37°C, and interacts with and partially stabilizes FNIP1/2 (Table 1). Thus, a slight structural stabilization conveyed by lowering the temperature is enough for this variant to evade the PQC-mediated clearance. Accordingly, we reasoned that perhaps the tumor suppressor function of some FLCN variants could be restored upon lowering the temperature. We

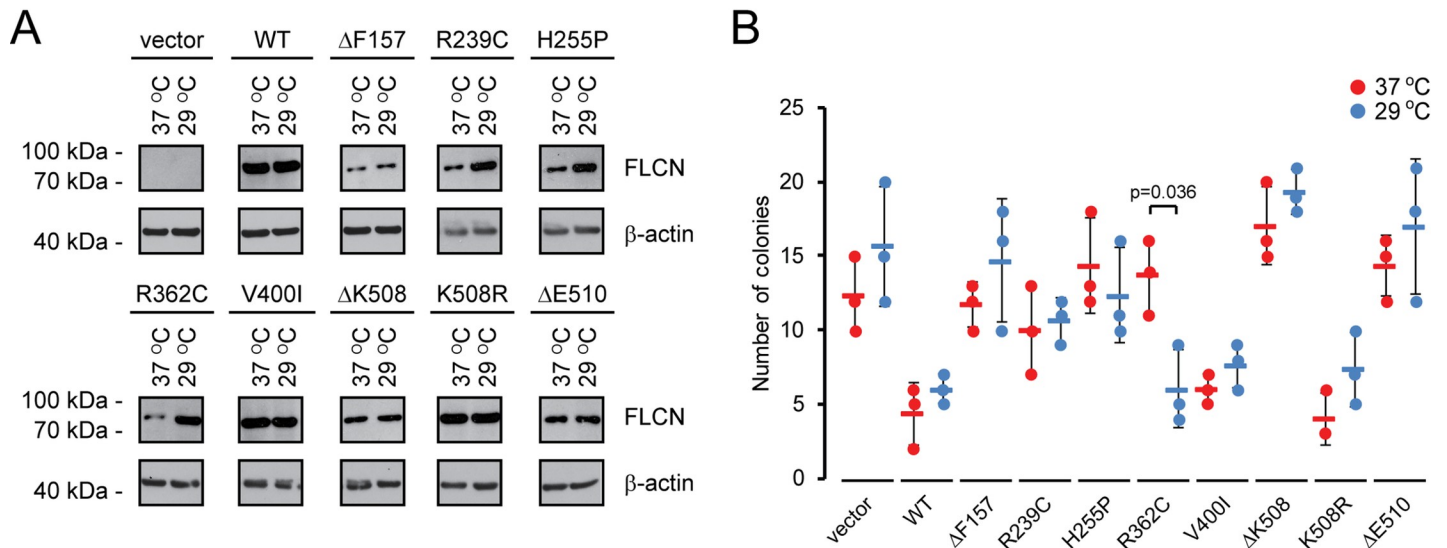


Fig 7. BHD-linked FLCN variants are stabilized at reduced temperatures. (A) The steady-state level of wild-type (WT) FLCN and the selected FLCN variants, expressed in U2OS cells, was compared at 37°C and 29°C. FLCN was detected using antibodies to FLCN. β -actin served as a loading control. (B) Colony formation at 37°C (red) and 29°C (blue) of FTC-133 cells transfected with the indicated expression constructs. The bars indicate the standard deviation ($n = 3$, p -value based on students t-test).

<https://doi.org/10.1371/journal.pgen.1009187.g007>

therefore investigated the ability of the FLCN variants to suppress the growth of *FLCN*-negative FTC-133 cells suspended in soft agar at 37°C and 29°C. The FLCN expression constructs were transfected into FTC-133 cells as stable mixed cell populations, and after four weeks at 37°C or 29°C colonies were counted. Wild-type FLCN led to roughly 50% reduction in colony formation at both temperatures (Fig 7B). The stable variants, V400I and K508R, both behaved like wild type and suppressed growth to a level similar to wild-type FLCN (Fig 7B). In line with a stabilization at low temperature, the R362C variant significantly reduced colony formation only at 29°C (Fig 7B), which was not apparent for any of the other FLCN variants. Presumably the other destabilized FLCN variants are subject to more dramatic structural effects causing FLCN misfolding to an extent where the proteins cannot attain their native conformation and will thus not be functional when the temperature is lowered or if the degradation was blocked.

Discussion

According to the ClinVar database [85], most disease-linked *FLCN* variants in the coding regions are frameshift mutations leading to C-terminal truncations of the FLCN protein (S10 Fig.). In the gnomAD database containing more than 100,000 exome sequences, some *FLCN* frameshift variants are also reported, but as expected these are exceedingly rare in the general population (S10 Fig.). In this work, we focus on the rare *FLCN* missense and single codon deletion variants linked to BHD syndrome.

Certainly, point mutations may directly ablate protein function without grossly affecting protein structure, e.g. by disrupting the active site of an enzyme. More commonly, however, missense mutations or in-frame deletions result in a structural perturbation or destabilization of the encoded protein [68], and indeed a previous report has shown that several BHD-linked single site FLCN variants are destabilized [65]. The results presented here are perfectly in line with this observation, supported by structural modelling (Fig 2, S11 Fig.), and show that the structural destabilization, conferred by the mutations, leads to rapid proteasomal degradation

of the FLCN variants, and in the rare cases that BHD syndrome is triggered by such single site mutations, the disease should be considered a protein misfolding disease.

We found that some of the FLCN variants are mislocalized in cells and one variant ($\Delta E510$) formed perinuclear protein aggregates, suggesting that at least this variant is highly misfolded. Often, aggregated proteins are cleared by autophagy. However, similar to aggregation-prone variants of VHL [79], ataxin-3 [86] and DJ-1 [76], the FLCN $\Delta E510$ protein appeared to be entirely degraded via the proteasome, which suggests that molecular chaperones may dissolve the $\Delta E510$ aggregates prior to degradation.

Our screen in yeast cells revealed two oppositely acting regulators of FLCN stability. In agreement with chaperones playing a role in FLCN turnover, deletion of the Ydj1 co-chaperone led to a stabilization of the FLCN $\Delta E510$ variant. Deletion of the Ubp15, on the other hand, destabilized the FLCN $\Delta E510$ variant. This observation fits with Ubp15/USP7 possessing deubiquitylating activity, which by catalyzing the removal of ubiquitin chains from proteins destined for the proteasome counters the degradation. Previous studies have identified numerous binding partners and substrates of USP7 [84, 87], including p53, p16^{INK4a} and WASH [88–91]. Typically, these interact with USP7 through its TRAF domain and/or the UBL1/2 domains, and consensus motifs in USP7-binding partners have been described [84]. We note that FLCN contains multiple of these potential TRAF- and UBL1/2-domain binding consensus motifs, which could mediate direct interaction to USP7. However, notably USP7 appears to preferentially interact with E3 ubiquitin-protein ligases [84], as exemplified by the effect of USP7 on p53. Hence, in case of p53, USP7 has been shown to deubiquitylate and stabilize the E3 MDM2, which in turn leads to an increased degradation of p53 [90–93]. Presumably since PQC E3s display overlapping substrate specificity and are highly redundant [94, 95] our screen failed to uncover the E3(s) that target FLCN for degradation, and our results on USP7 suggest that USP7 directly deubiquitylates FLCN, rather than targeting an FLCN-specific E3.

In our experiments, we have relied on transient overexpression of FLCN variants. It is possible that different PQC system operate depending on the expression level of the misfolded protein, but to our knowledge this has not been systematically tested, and we cannot rule out that endogenous FLCN variants are targeted for degradation via a different PQC pathway. However, since we observe degradation of the FLCN variants that are predicted to be destabilized, it is unlikely that the overexpression is saturating the molecular chaperones or other PQC components in our experimental setup.

Classically, molecular chaperones are viewed as protein folding machines that capture non-native proteins and, through cycles of binding and release, catalyze folding into the correct native state. However, chaperones also directly interact and collaborate with components of the ubiquitin-proteasome system [2, 10, 15, 94, 96, 97]. For instance, HSP70 and HSP90 directly associate with the E3 ubiquitin ligase, CHIP, which in turn ubiquitylates the chaperone clients to ensure their degradation [4, 98]. Recently, it was shown that also wild-type FLCN is a HSP90 client protein and the FNIP1/2 binding partners function as co-chaperones that facilitate FLCN folding and ensure FLCN stability [52, 53]. Our finding that the yeast Hsp40 co-chaperone Ydj1 regulates the stability of the FLCN $\Delta E510$ variant could be relevant also for the stability of wild-type FLCN, and more detailed studies on the potential interplay between Hsp40s and FNIP1/2 in FLCN folding and stability are warranted. Since some co-chaperones, including Ydj1 [99], appear to play an active role in degradation, it is possible that the co-chaperones regulate whether FLCN is folded or degraded. In our assays, we observed that FLCN also functions to stabilize FNIP1/2, and this stabilization depends on FNIP1/2 interaction. Hence, for those FLCN variants that are misfolded and fail to interact with FNIP1/2, the FNIP1/2 levels are reduced, due to proteasomal degradation. Subunits in multiprotein assemblies are generally more stable once incorporated into a complex and unassembled (orphan)

proteins, produced in excess, are targeted for degradation [100, 101]. Hence, our observation that FLCN stabilizes FNIP1/2 are in line with earlier reports showing that FNIP1/2 stabilize FLCN [52, 59, 60]. The observation of such mutually stabilizing effects confirms that FLCN forms a stable complex with FNIP1/2. However, in case of FLCN and FNIP1/2, the balance in their stoichiometry might also be regulated by environmental cues. Indeed, it was recently shown that in the presence of nutrients, FNIP2 is phosphorylated by casein kinase 1 (CK1) and degraded by the proteasome [102]. The experiments, presented here, were also performed under nutrient-rich conditions, and it is possible that the observed degradation of FNIP1/2 is triggered by CK1 phosphorylation of orphan FNIP1/2.

Intriguingly, we observed a clear correlation between the degradation rate of the unstable variants and several of the other tested parameters. Thus, all the unstable variants displayed reduced solubility, and with the exception of R239C and R362C, the unstable FLCN variants were all exclusively localized in the cytosol and failed to associate with and stabilize FNIP1 and FNIP2 (Table 1).

Of the tested FLCN variants, only two, V400I and K508R, behaved like wild-type FLCN with regard to level, turnover, interaction, localization and cell proliferation (Table 1). Since valine/isoleucine and lysine/arginine, are, respectively, chemically similar amino acids, it is not surprising that these substitutions do not render FLCN structurally unstable. However, importantly, these findings do not preclude that the V400I and K508R variants are pathogenic. According to the gnomAD database [77], both of the V400I and K508R variants are rare (minor allele frequencies ca. ~1:40,000 and 1:5,000, respectively). The estimated prevalence of BHD syndrome according to the Orphanet database is 1:200,000, suggesting that if the K508R mutation is pathogenic, it is likely to have a reduced penetrance. ClinVar lists K508R as likely benign [85]. However, a recent report has shown that although introducing the K508R variant in *Fln* knock-out mice prolonged survival, the mice later developed cystic kidneys and succumbed to renal failure [103], indicating that K508R might be a weakly pathogenic mutation. It is possible that the slow onset, observed for the K508R mouse model, is connected with the K508R variant being only slightly more unstable than wild-type FLCN *in vivo*. However, it is more likely that any potential pathogenicity associated with the V400I and K508R variants, is not caused by structural destabilization, but instead associated with other properties of the FLCN protein that we did not test here.

Since we found that several of the variants were stabilized by lowering the temperature, these proteins are probably not highly destabilized or misfolded. Indeed, for the R362C variant, we observed an increased cellular function when the temperature was reduced. Thus, similar to other genetic diseases, including cystic fibrosis [104] and von Hippel-Lindau disease [105], as well as certain cancer-linked mutations in p53 [106], it may be possible to stabilize some misfolded FLCN protein variants using a small molecule that either blocks the PQC system or directly stabilizes the FLCN protein structure [107]. However, to achieve this it is essential with further, in particular structural and biophysical, studies of both wild-type and disease-linked FLCN protein variants. Finally, the structural stability predictions that we describe here may be useful in diagnostics of BHD syndrome in the rare cases where missense variants or single residue deletions are observed.

Materials and methods

Buffers

Buffer A: 50 mM Tris/HCl pH 7.4, 150 mM NaCl, 1 mM EDTA, 0.5% NP-40, 1 mM PMSF and Complete protease inhibitors (Roche). Buffer B: 50 mM Tris/HCl pH 7.4, 1 mM EDTA, 150 mM NaCl, 1 mM PMSF and Complete protease inhibitors (Roche). PBS: 10 mM Na₂HPO₄, 1.8 mM KH₂PO₄, 137 mM NaCl, 3 mM KCl, pH 7.4.

Plasmids

Full-length wild-type human *FLCN* cDNA carrying an N-terminal RGS6xHis-tag was expressed from pcDNA3.1 (Genscript). USP7 was expressed with an N-terminal myc-tag from pcDNA3.1 (Genscript). All mutations were generated by Genscript. The pcDNA3.1-FLAG-FNIP1 and the pcDNA3.1+N-eGFP-*FLCN*ΔE510 vectors were generated by Genscript. The pIRES2-*FLCN* plasmids were kindly provided by Dr. E. R. Maher (Birmingham, UK). The pEGFP-N1-*FLCN*, pRK5-HA-FNIP1 and pRK5-HA-FNIP2 constructs were kindly provided by Dr. D. M. Sabatini (MIT, USA).

Cell culture

U2OS cells (ATCC) were propagated in Dulbecco's Modified Eagle medium (DMEM) with 10% fetal-calf serum (Invitrogen), and supplemented with 5000 IU/mL penicillin, 5 mg/mL streptomycin and 2 mM glutamine at 37°C. FTC-133 cells (ECACC) were similarly cultured but in DMEM:Ham's F12 (1:1) medium with 2 mM glutamine and 10% fetal-calf serum (Invitrogen). FugeneHD (Promega) was used for transfections following the manufacturer's instructions. Cell imaging and quantifications were performed as described before [11]. Protein aggregates were counted manually.

Electrophoresis and blotting

Unless otherwise stated whole cell extracts were prepared by lysing cells directly in SDS sample buffer. SDS-PAGE was performed on 12.5% acrylamide gels. For Western blotting 0.2 μm nitrocellulose membranes were used. For blocking, the membranes were incubated in 5% fat-free milk powder and 0.1% Tween-20 in PBS. Antibodies and their sources were: anti-ubiquitin (Z0458, DAKO), anti-Rpt6 (p45-110, Enzo Biosciences), anti-20S proteasome α-subunits (MCP231, Enzo Biosciences), anti-*FLCN* (D14G9, Cell Signaling Technology), anti-GFP (3H9, Chromotek), anti-myc (9E1, Chromotek) anti-HA (12CA5, Roche), anti-Flag (M2, Sigma), anti-RGSHis (34650, Qiagen), anti-β-actin (AC74, Sigma), anti-NaK-ATPase (C464.6, Sigma), anti-LC3A/B (D3U4C, Cell Signaling Technology), anti-GAPDH (14C10, Cell Signaling Technology), anti-α tubulin (TAT-1, 00020911 Sigma). All secondary antibodies were purchased from DAKO. The Un-Scan-It v6.1 software (Silk Scientific) was used for densitometry.

Protein degradation experiments

Bortezomib (LC Laboratories) and chloroquine (Sigma) were used at 15 μM and 20 μM respectively, for 8 hours in serum-free media. Degradation was followed in cultures treated with cycloheximide (CHX) as described previously [11].

Co-precipitation experiments

Binding studies were performed as described before [11], using anti-HA resin (Sigma) or myc-trap beads (Chromotek). Bound proteins were eluted directly in SDS sample buffer.

FLCN solubility

To estimate the solubility of the *FLCN* variants, a confluent 6-well dish of transfected U2OS cells was lysed in 200 μL buffer B by three 20 second rounds of sonication on ice. The lysate was then centrifuged at 15000 g for 30 minutes at 4°C. Finally, 4x concentrated SDS sample buffer was added to the supernatant to obtain a 1x SDS sample buffer lysate. The pellet was resuspended in 1x SDS sample buffer to match the volume of the supernatant.

Filter trap assays

Filter trap assays were performed largely as described previously [80]. Briefly, to achieve equal cellular expression of wild-type FLCN and FLCN Δ 510 protein, the plasmid encoding wild-type FLCN was diluted with empty control vector prior to transfection. Transfected cells were harvested in ice-cold PBS using a cell scraper and lysed by sonication for three times 10 seconds in ice-cold PBS containing Complete protease inhibitors (Roche). Unbroken cells were removed by centrifugation at 500 g for 2 minutes. SDS was added to a final concentration of 2% and three two-fold serial dilutions in 2% SDS in PBS were prepared. Samples of 200 μ L were loaded onto a 0.2 μ m nitrocellulose membrane affixed in a BioRad Bio-Dot apparatus (BioRad) pre-equilibrated with 100 μ L PBS per well. The wells were then washed once with 400 μ L 2% SDS in PBS and then once with 200 μ L 2% SDS in PBS. The nitrocellulose membrane was then removed from the apparatus and washed briefly in PBS, before blocking and development as a Western blot using antibodies to FLCN and as a control GAPDH.

Soft agar colony formation assays

Soft agar colony formation assays were performed as described [65] using pools of FTC-133 cells stably transfected to express the FLCN variants. After four weeks, colonies greater than 100 μ m in diameter were counted. The experiments were performed in triplicates.

Yeast strains and techniques

All yeast strains were from the Euroscarf collection and transformations were performed using lithium acetate [108]. For analyzing growth on solid media, exponential phase cultures were diluted to an OD_{600nm} of 0.40 and 5 μ L of 5-fold serial dilutions were applied in spots on agar plates. Cell extracts for Western blotting were prepared with glass beads in trichloroacetic acid (Sigma) as described [109]. Cycloheximide (CHX) (Sigma) was used at a concentration of 100 μ g/mL. Bortezomib (BZ) (LC Laboratories) was used at a concentration of 1 mM. The screening of the yeast gene deletion library [83] was performed by first transforming the FLCN-Ura3 reporter plasmid (pTR1412-FLCN Δ E510) into the query strain Y7092 (*MAT α can1 Δ ::STE2pr-Sp_his5 lyp1 Δ ura3 Δ 0 leu2 Δ 0 his3 Δ 1 met15 Δ 0 geneX::KanMX6*) and selecting transformants on SC-Leu medium. Next, the transformed strain was mated to the yeast gene deletion strain collection by automated pinning (RoToR, Singer Instruments, UK). Selection for diploids, sporulation, and selection for haploid progeny containing the gene deletion (G418^R) and the FLCN-Ura3 reporter plasmid was performed essentially as described [110].

Calculation of $\Delta\Delta$ Gs for missense variants

We used the Rosetta cartesian_ddg protocol [73] and the high-resolution structure of the C-terminal FLCN domain (PDB 3V42) [54] to calculate $\Delta\Delta$ Gs for missense variants, as also previously described [12]. Three iterations were performed for each of the 20 possible amino acid variants at each position, including the wild type for reference. The value reported here is the difference between the average of the wild-type Rosetta energies and the average for the respective variant. All scores are divided by 2.9 to bring them to a kcal/mol scale (Frank DiMaio, personal communication).

$\Delta\Delta$ Gs for in-frame deletion variants

First 25 homology models were created [111] for each single-amino-acid-deletion in the C-terminal domain, using PDB 3V42 [54] as the template. Each homology model was relaxed in two independent trajectories using the command line:

```
/path/to/rosetta/source/bin/relax.linuxgccrelease /  
-database /path/to/rosetta/database \  
-l list_w_models.lst  
-ignore_unrecognized_res -use_input_sc -constrain_relax_to_start_coords  
-flip_HNQ -no_optH false -relax:fast -nstruct 2
```

based on Jackson et al. [75]. The median of the resulting 50 scores was calculated to estimate the ΔG (in Rosetta Energy Units) of the respective deletion variant. To estimate $\Delta\Delta G$ s of in-frame deletions, the 10th percentile of the ΔG distribution was subtracted. Analogous to the missense variant $\Delta\Delta G$ s above, scores were divided by 2.9 to bring them to a scale that corresponds to kcal/mol.

Supporting information

S1 Fig. Endogenous FLCN in U2OS cells is stable. The level of endogenous FLCN in U2OS cells was analyzed by Western blotting of whole cell lysates, using antibodies to FLCN, in cultures that were either untreated (-) or treated with bortezomib (+BZ) or cycloheximide (+CHX) for 8 hours. β -actin served as a loading control. (JPG)

S2 Fig. The FLCN variants are not autophagy targets. The steady-state levels of the FLCN variants were compared by Western blotting of whole cell lysates, using antibodies to FLCN, in cultures that were either untreated or treated with the autophagy inhibitor chloroquine (CQ) for 8 hours. β -actin served as a loading control, while blotting for the autophagy substrate, LC3, was included as a control for successful inhibition of autophagy. (JPG)

S3 Fig. Several BHD-linked FLCN variants are insoluble. (A) The solubility of the selected FLCN variants. Samples of whole cell lysates were separated into a soluble supernatant (S) fraction and an insoluble pellet (P) fraction by centrifugation. FLCN concentrations were determined by SDS-PAGE and Western blotting with antibodies to FLCN. Na/K ATPase and β -actin were used as loading controls. (B) Quantification of blots as shown in (A) by densitometry. The soluble fractions are shown in dark grey, the insoluble pellet fractions in light grey. For quantification the faster migrating band was included. The error bars show the standard deviation ($n = 3$). (JPG)

S4 Fig. The subcellular localization of FLCN is unchanged by proteasome inhibition. U2OS cells transiently transfected to express 6His-tagged wild type FLCN and selected FLCN variants were treated with the proteasome inhibitor bortezomib (BZ) for 8 hours and analyzed by fluorescence microscopy. FLCN was stained using antibodies to the 6His-tag, and Hoechst was used to mark the nucleus. (JPG)

S5 Fig. FNIP1/2 are proteasome targets in the absence of FLCN. The level of overexpressed HA-tagged FNIP1 and FNIP2 in U2OS cells was analyzed by Western blotting of whole cell lysates, using antibodies to the HA-tag, in cultures that were either left untreated (-) or treated (+) with bortezomib (BZ) for 8 hours. β -actin served as a loading control. (JPG)

S6 Fig. Analyses of the FLCN H429Pfs variant. (A) The FLCN H429Pfs variant leads to addition of the shown residues before terminating (boxed sequence). The structure of the FLCN-FNIP2 complex is shown based on the recently resolved cryo-EM structure of FLCN (coloured) and FNIP2 (gray) (PDB 6ULG) (Shen et al., 2019). The purple region is missing in the H429Pfs variant. (B) U2OS cells were transiently transfected to express either wt FLCN or H429Pfs, with or without expression of HA-tagged FNIP1 as indicated. Then the levels of FLCN and FNIP1 in whole cell lysates were compared by SDS-PAGE and Western blotting with antibodies to FLCN or the HA-tag on FNIP1. β -actin served as a loading control. (C) U2OS cells were transiently transfected to express either wt FLCN or H429Pfs, with or without expression of HA-tagged FNIP2 as indicated. Then the levels of FLCN and FNIP2 in whole cell lysates were compared by SDS-PAGE and Western blotting with antibodies to FLCN or the HA-tag on FNIP2. β -actin served as a loading control. (D) U2OS cells were transiently transfected to express either vector, wt FLCN or H429Pfs, and HA-tagged FNIP1 or FNIP2 as indicated, and treated with bortezomib (+BZ) for 8 hours. Cleared extracts (input) were prepared and used for immunoprecipitation (IP) using antibodies to the HA-tag on FNIP1/2. Finally, the samples were resolved by SDS-PAGE and analyzed by Western blotting with antibodies to FLCN or the HA-tag on FNIP1/2, and as a control to β -actin. (E) The level of transfected H429Pfs in U2OS was compared upon co-transfection with myc-tagged USP7 and the catalytically dead USP7 variant (C223A) by Western blotting of whole cell lysates. FLCN was detected using the antibody to FLCN. USP7 was detected by using antibodies to the myc-tag. Probing for β -actin was included as a control.

(JPG)

S7 Fig. FLCN contains multiple potential USP7 interaction motifs. The figure depicts the amino acid sequence of FLCN with the USP7 UBL1/2 (yellow) and TRAF recognition motifs (cyan) marked. The consensus sequences as defined by Kim and Sixma (Kim and Sixma, 2017) of the recognition motifs is given below. The x denotes any amino acid residue.

(JPG)

S8 Fig. The potential USP7 binding sites in the FLCN structure. Mapping of the putative USP7 binding sites to the recently resolved cryo-EM structure of FLCN (PDB 6ULG) (Shen et al., 2019) with FLCN in magenta and FNIP2 in gray. Only 3 of the 10 putative sites correspond to regions that are resolved in the structure, namely 236AARS, 264ACGS, which are both in the N-terminal domain, and the UBL1/2 recognition motif (KVKVLFK) in the C-terminal domain. Two of these sites are covered by interaction interfaces with FNIP2 and are thus likely not accessible unless the complexes dissociates. Color coding of motifs as in [S7 Fig.](#)

(JPG)

S9 Fig. Normal appearance of the ubiquitin-proteasome system at 29°C. The levels of ubiquitin-protein conjugates and 26S proteasomes in whole cell lysates was compared between U2OS cells grown at 29°C and at 37°C by blotting for ubiquitin, the 19S regulatory complex subunit Rpt6 and the 20S proteasome α -subunits. β -actin served as a loading control.

(JPG)

S10 Fig. FLCN variants reported in ClinVar and gnomAD. (A) Distribution of missense, frameshift and deletion variants in *FLCN* coding regions listed in ClinVar. Blue, benign. Red, pathogenic. (B) Allele frequency and distribution of the *FLCN* variants reported in gnomAD. Purple, frameshift. Yellow, inframe deletion. Grey, missense.

(JPG)

S11 Fig. Modelling of the R362C and Δ E510 variants. (A) The FLCN R362 residue forms H-bonds with the sidechain of N484 and possibly the backbone carbonyl-O of L483. Accordingly, R362C substitution is expected to be destabilizing, since a C at this position will be unable to engage in these interactions. (B) Introducing a deletion at position E510 is likely to distort the following part of the helix. The models are based on the FLCN crystal structure (PDB: 3V42). (JPG)

S1 Dataset. *In silico* saturation mutagenesis data.
(XLSX)

S2 Dataset. Results from the yeast screen.
(XLSX)

S3 Dataset. Numerical data.
(XLSX)

Acknowledgments

The authors thank Dr. Thomas Hansen, Dr. Elin Pietras, Dr. Cornelia Steinhauer, Rasmus Scheller, Sven Larsen-Ledet and Anne-Marie Lauridsen for excellent technical assistance, and Dr. Thomas van Overeem Hansen and Dr. Klavs B. Hendil for helpful discussions and comments on the manuscript. We acknowledge Dr. Elena Papaleo, who contributed to early parts of this project. We thank Dr. Charlie Boone for sharing reagents. Expression plasmids were kindly provided by Dr. David M. Sabatini and Dr. Eamonn R. Maher.

Author Contributions

Conceptualization: Kresten Lindorff-Larsen, Rasmus Hartmann-Petersen.

Formal analysis: Lene Clausen, Amelie Stein, Sofie V. Nielsen, Michael Lisby, Tommer Ravid, Kresten Lindorff-Larsen, Rasmus Hartmann-Petersen.

Investigation: Lene Clausen, Amelie Stein, Martin Grønbaek-Thygesen, Lasse Nygaard, Cecilie L. Søltøft, Sofie V. Nielsen.

Methodology: Michael Lisby, Tommer Ravid.

Supervision: Michael Lisby, Tommer Ravid, Kresten Lindorff-Larsen, Rasmus Hartmann-Petersen.

Writing – original draft: Lene Clausen.

Writing – review & editing: Lene Clausen, Amelie Stein, Kresten Lindorff-Larsen, Rasmus Hartmann-Petersen.

References

1. Hartl FU, Bracher A, Hayer-Hartl M. Molecular chaperones in protein folding and proteostasis. *Nature*. 2011; 475:324–332. <https://doi.org/10.1038/nature10317> PMID: 21776078
2. Kriegenburg F, Ellgaard L, Hartmann-Petersen R. Molecular chaperones in targeting misfolded proteins for ubiquitin-dependent degradation. *FEBS J*. 2012; 279:532–542. <https://doi.org/10.1111/j.1742-4658.2011.08456.x> PMID: 22177318
3. Jones RD, Gardner RG. Protein quality control in the nucleus. *Curr Opin Cell Biol*. 2016; 40:81–89. <https://doi.org/10.1016/j.ceb.2016.03.002> PMID: 27015023
4. Esser C, Alberti S, Hohfeld J. Cooperation of molecular chaperones with the ubiquitin/proteasome system. *Biochim Biophys Acta*. 2004; 1695:171–188. <https://doi.org/10.1016/j.bbamcr.2004.09.020> PMID: 15571814

5. Sontag EM, Vonk WI, Frydman J. Sorting out the trash: the spatial nature of eukaryotic protein quality control. *Curr Opin Cell Biol.* 2014; 26C:139–146. <https://doi.org/10.1016/j.ceb.2013.12.006> PMID: 24463332
6. Amm I, Sommer T, Wolf DH. Protein quality control and elimination of protein waste: the role of the ubiquitin-proteasome system. *Biochim Biophys Acta.* 2014; 1843:182–196. <https://doi.org/10.1016/j.bbamcr.2013.06.031> PMID: 23850760
7. Shiber A, Ravid T. Chaperoning proteins for destruction: diverse roles of Hsp70 chaperones and their co-chaperones in targeting misfolded proteins to the proteasome. *Biomolecules.* 2014; 4:704–724.
8. Kevei E, Pokrzywa W, Hoppe T. Repair or destruction—an intimate liaison between ubiquitin ligases and molecular chaperones in proteostasis. *FEBS Lett.* 2017; 591:2616–2635. <https://doi.org/10.1002/1873-3468.12750> PMID: 28699655
9. Geffen Y, Appleboim A, Gardner RG, Friedman N, Sadeh R, Ravid T. Mapping the Landscape of a Eukaryotic Degronome. *Mol Cell.* 2016; 63:1055–1065. <https://doi.org/10.1016/j.molcel.2016.08.005> PMID: 27618491
10. Maurer MJ, Spear ED, Yu AT, Lee EJ, Shahzad S, Michaelis S. Degradation Signals for Ubiquitin-Proteasome Dependent Cytosolic Protein Quality Control (CytoQC) in Yeast. *G3 (Bethesda).* 2016; 6:1853–1866. <https://doi.org/10.1534/g3.116.027953> PMID: 27172186
11. Nielsen SV, Stein A, Dinitzen AB, Papaleo E, Tatham MH, Poulsen EG et al. Predicting the impact of Lynch syndrome-causing missense mutations from structural calculations. *PLoS Genet.* 2017; 13: e1006739. <https://doi.org/10.1371/journal.pgen.1006739> PMID: 28422960
12. Scheller R, Stein A, Nielsen SV, Marin FI, Gerdes AM, Di MM et al. Toward mechanistic models for genotype-phenotype correlations in phenylketonuria using protein stability calculations. *Hum Mutat.* 2019; 40:444–457. <https://doi.org/10.1002/humu.23707> PMID: 30648773
13. Abildgaard AB, Stein A, Nielsen SV, Schultz-Knudsen K, Papaleo E, Shrikhande A et al. Computational and cellular studies reveal structural destabilization and degradation of MLH1 variants in Lynch syndrome. *Elife.* 2019; 8. <https://doi.org/10.7554/eLife.49138> PMID: 31697235
14. Gardner RG, Nelson ZW, Gottschling DE. Degradation-mediated protein quality control in the nucleus. *Cell.* 2005; 120:803–815. <https://doi.org/10.1016/j.cell.2005.01.016> PMID: 15797381
15. Kriegenburg F, Jakopc V, Poulsen EG, Nielsen SV, Roguev A, Krogan N et al. A chaperone-assisted degradation pathway targets kinetochore proteins to ensure genome stability. *PLoS Genet.* 2014; 10: e1004140. <https://doi.org/10.1371/journal.pgen.1004140> PMID: 24497846
16. Kampmeyer C, Karakostova A, Schenstrom SM, Abildgaard AB, Lauridsen AM, Jourdain I et al. The exocyst subunit Sec3 is regulated by a protein quality control pathway. *J Biol Chem.* 2017; 292:15240–15253. <https://doi.org/10.1074/jbc.M117.789867> PMID: 28765280
17. Meacham GC, Patterson C, Zhang W, Younger JM, Cyr DM. The Hsc70 co-chaperone CHIP targets immature CFTR for proteasomal degradation. *Nat Cell Biol.* 2001; 3:100–105. <https://doi.org/10.1038/35050509> PMID: 11146634
18. Ahner A, Nakatsukasa K, Zhang H, Frizzell RA, Brodsky JL. Small heat-shock proteins select deltaF508-CFTR for endoplasmic reticulum-associated degradation. *Mol Biol Cell.* 2007; 18:806–814. <https://doi.org/10.1091/mbc.e06-05-0458> PMID: 17182856
19. Arora S, Huwe PJ, Sikder R, Shah M, Browne AJ, Lesh R et al. Functional analysis of rare variants in mismatch repair proteins augments results from computation-based predictive methods. *Cancer Biol Ther.* 2017; 18:519–533. <https://doi.org/10.1080/15384047.2017.1326439> PMID: 28494185
20. McCafferty CL, Sergeev YV. In silico Mapping of Protein Unfolding Mutations for Inherited Disease. *Sci Rep.* 2016; 6:37298. <https://doi.org/10.1038/srep37298> PMID: 27905547
21. Kumar V, Rahman S, Choudhry H, Zamzami MA, Sarwar JM, Islam A et al. Computing disease-linked SOD1 mutations: deciphering protein stability and patient-phenotype relations. *Sci Rep.* 2017; 7:4678. <https://doi.org/10.1038/s41598-017-04950-9> PMID: 28680046
22. Wagih O, Galardini M, Busby BP, Memon D, Typas A, Beltrao P. A resource of variant effect predictions of single nucleotide variants in model organisms. *Mol Syst Biol.* 2018; 14:e8430.
23. Beaver SK, Mesa-Torres N, Pey AL, Timson DJ. NQO1: A target for the treatment of cancer and neurological diseases, and a model to understand loss of function disease mechanisms. *Biochim Biophys Acta Proteins Proteom.* 2019; 1867:663–676. <https://doi.org/10.1016/j.bbapap.2019.05.002> PMID: 31091472
24. Caswell RC, Owens MM, Gunning AC, Ellard S, Wright CF. Using Structural Analysis In Silico to Assess the Impact of Missense Variants in MEN1. *J Endocr Soc.* 2019; 3:2258–2275. <https://doi.org/10.1210/je.2019-00260> PMID: 31737856

25. Iqbal S, Jespersen JB, Perez-Palma E, May P, Hoksza D, Heyne HO et al. Insights into protein structural, physicochemical, and functional consequences of missense variants in 1,330 disease-associated human genes. *bioRxiv*. 2019;693259.
26. Tang N, Sandahl T, Ott P, Kepp KP. Benchmarking Computational Methods for Estimating the Pathogenicity of Wilson's Disease Mutations *bioRxiv* 2019;780924:
27. Jepsen MM, Fowler DM, Hartmann-Petersen R, Stein A, Lindorff-Larsen K. Classifying disease-associated variants using measures of protein activity and stability. *bioRxiv*. 2019;688234.
28. Tiberti M, Terkelsen T, Cremers TC, Di Marco M, da Piedade I, Maiani E et al. MutateX: an automated pipeline for *in-silico* saturation mutagenesis of protein structures and structural ensembles. *bioRxiv*. 2019;824938.
29. Casadio R, Vassura M, Tiwari S, Fariselli P, Luigi MP. Correlating disease-related mutations to their effect on protein stability: a large-scale analysis of the human proteome. *Hum Mutat*. 2011; 32:1161–1170. <https://doi.org/10.1002/humu.21555> PMID: 21853506
30. Pal LR, Moulton J. Genetic Basis of Common Human Disease: Insight into the Role of Missense SNPs from Genome-Wide Association Studies. *J Mol Biol*. 2015; 427:2271–2289.
31. Nickerson ML, Warren MB, Toro JR, Matrosova V, Glenn G, Turner ML et al. Mutations in a novel gene lead to kidney tumors, lung wall defects, and benign tumors of the hair follicle in patients with the Birt-Hogg-Dube syndrome. *Cancer Cell*. 2002; 2:157–164. [https://doi.org/10.1016/s1535-6108\(02\)00104-6](https://doi.org/10.1016/s1535-6108(02)00104-6) PMID: 12204536
32. Zbar B, Alvord WG, Glenn G, Turner M, Pavlovich CP, Schmidt L et al. Risk of renal and colonic neoplasms and spontaneous pneumothorax in the Birt-Hogg-Dube syndrome. *Cancer Epidemiol Biomarkers Prev*. 2002; 11:393–400. PMID: 11927500
33. Schmidt LS, Linehan WM. FLCN: The causative gene for Birt-Hogg-Dube syndrome. *Gene*. 2018; 640:28–42. <https://doi.org/10.1016/j.gene.2017.09.044> PMID: 28970150
34. Birt AR, Hogg GR, Dube WJ. Hereditary multiple fibrofolliculomas with trichodiscomas and acrochordons. *Arch Dermatol*. 1977; 113:1674–1677. PMID: 596896
35. Menko FH, van Steensel MA, Giraud S, Friis-Hansen L, Richard S, Ungari S et al. Birt-Hogg-Dube syndrome: diagnosis and management. *Lancet Oncol*. 2009; 10:1199–1206. [https://doi.org/10.1016/S1470-2045\(09\)70188-3](https://doi.org/10.1016/S1470-2045(09)70188-3) PMID: 19959076
36. Toro JR, Glenn G, Duray P, Darling T, Weirich G, Zbar B et al. Birt-Hogg-Dube syndrome: a novel marker of kidney neoplasia *Arch Dermatol* 1999; 135:1195–1202. <https://doi.org/10.1001/archderm.135.10.1195> PMID: 10522666
37. Kovacs D, Kalmar E, Torok Z, Tompa P. Chaperone activity of ERD10 and ERD14, two disordered stress-related plant proteins. *Plant Physiol*. 2008; 147:381–390. <https://doi.org/10.1104/pp.108.118208> PMID: 18359842
38. Khoo SK, Bradley M, Wong FK, Hedblad MA, Nordenskjold M, Teh BT. Birt-Hogg-Dube syndrome: mapping of a novel hereditary neoplasia gene to chromosome 17p12-q11.2. *Oncogene*. 2001; 20:5239–5242. <https://doi.org/10.1038/sj.onc.1204703> PMID: 11526515
39. Schmidt LS, Warren MB, Nickerson ML, Weirich G, Matrosova V, Toro JR et al. Birt-Hogg-Dube syndrome, a genodermatosis associated with spontaneous pneumothorax and kidney neoplasia, maps to chromosome 17p11.2. *Am J Hum Genet*. 2001; 69:876–882. <https://doi.org/10.1086/323744> PMID: 11533913
40. Vocke CD, Yang Y, Pavlovich CP, Schmidt LS, Nickerson ML, Torres-Cabala CA et al. High frequency of somatic frameshift BHD gene mutations in Birt-Hogg-Dube-associated renal tumors. *J Natl Cancer Inst*. 2005; 97:931–935. <https://doi.org/10.1093/jnci/dji154> PMID: 15956655
41. Yang Y, Padilla-Nash HM, Vira MA, Abu-Asab MS, Val D, Worrell R et al. The UOK 257 cell line: a novel model for studies of the human Birt-Hogg-Dube gene pathway. *Cancer Genet Cytogenet*. 2008; 180:100–109. <https://doi.org/10.1016/j.cancergencyto.2007.10.010> PMID: 18206534
42. Okimoto K, Sakurai J, Kobayashi T, Mitani H, Hirayama Y, Nickerson ML et al. A germ-line insertion in the Birt-Hogg-Dube (BHD) gene gives rise to the Nihon rat model of inherited renal cancer. *Proc Natl Acad Sci U S A*. 2004; 101:2023–2027. <https://doi.org/10.1073/pnas.0308071100> PMID: 14769940
43. Togashi Y, Kobayashi T, Momose S, Ueda M, Okimoto K, Hino O. Transgenic rescue from embryonic lethality and renal carcinogenesis in the Nihon rat model by introduction of a wild-type Bhd gene. *Oncogene*. 2006; 25:2885–2889.
44. Lingaas F, Comstock KE, Kirkness EF, Sorensen A, Aarskaug T, Hitte C et al. A mutation in the canine BHD gene is associated with hereditary multifocal renal cystadenocarcinoma and nodular dermatofibrosis in the German Shepherd dog. *Hum Mol Genet*. 2003; 12:3043–3053. <https://doi.org/10.1093/hmg/ddg336> PMID: 14532326

45. Baba M, Furihata M, Hong SB, Tessarollo L, Haines DC, Southon E et al. Kidney-targeted Birt-Hogg-Dube gene inactivation in a mouse model: Erk1/2 and Akt-mTOR activation, cell hyperproliferation, and polycystic kidneys. *J Natl Cancer Inst.* 2008; 100:140–154.
46. Klomp JA, Petillo D, Niemi NM, Dykema KJ, Chen J, Yang XJ et al. Birt-Hogg-Dube renal tumors are genetically distinct from other renal neoplasias and are associated with up-regulation of mitochondrial gene expression. *BMC Med Genomics.* 2010; 3:59.
47. Hong SB, Oh H, Valera VA, Baba M, Schmidt LS, Linehan WM. Inactivation of the FLCN tumor suppressor gene induces TFE3 transcriptional activity by increasing its nuclear localization. *PLoS One.* 2010; 5:e15793. <https://doi.org/10.1371/journal.pone.0015793> PMID: 21209915
48. Napolitano G, Di MC, Esposito A, de Araujo MEG, Pece S, Bertalot G et al. A substrate-specific mTORC1 pathway underlies Birt-Hogg-Dubé syndrome. *Nature.* 2020. <https://doi.org/10.1038/s41586-020-2444-0> PMID: 32612235
49. Nahorski MS, Seabra L, Straatman-Iwanowska A, Wingenfeld A, Reiman A, Lu X et al. Folliculin interacts with p0071 (plakophilin-4) and deficiency is associated with disordered RhoA signalling, epithelial polarization and cytokinesis. *Hum Mol Genet.* 2012; 21:5268–5279. <https://doi.org/10.1093/hmg/ddc378> PMID: 22965878
50. Bar-Peled L, Sabatini DM. Regulation of mTORC1 by amino acids. *Trends Cell Biol.* 2014; 24:400–406. <https://doi.org/10.1016/j.tcb.2014.03.003> PMID: 24698685
51. Tsun ZY, Bar-Peled L, Chantranupong L, Zoncu R, Wang T, Kim C et al. The folliculin tumor suppressor is a GAP for the RagC/D GTPases that signal amino acid levels to mTORC1. *Mol Cell.* 2013; 52:495–505.
52. Woodford MR, Dunn DM, Blanden AR, Capriotti D, Loïselle D, Prodromou C et al. The FNIP co-chaperones decelerate the Hsp90 chaperone cycle and enhance drug binding. *Nat Commun.* 2016; 7:12037. <https://doi.org/10.1038/ncomms12037> PMID: 27353360
53. Sager RA, Woodford MR, Backe SJ, Makedon AM, Baker-Williams AJ, DiGregorio BT et al. Post-translational Regulation of FNIP1 Creates a Rheostat for the Molecular Chaperone Hsp90. *Cell Rep.* 2019; 26:1344–1356. <https://doi.org/10.1016/j.celrep.2019.01.018> PMID: 30699359
54. Nookala RK, Langemeyer L, Pacitto A, Ochoa-Montano B, Donaldson JC, Blaszczyk BK et al. Crystal structure of folliculin reveals a hidDENN function in genetically inherited renal cancer. *Open Biol.* 2012; 2:120071. <https://doi.org/10.1098/rsob.120071> PMID: 22977732
55. Wu X, Bradley MJ, Cai Y, Kummel D, De La Cruz EM, Barr FA et al. Insights regarding guanine nucleotide exchange from the structure of a DENN-domain protein complexed with its Rab GTPase substrate. *Proc Natl Acad Sci U S A.* 2011; 108:18672–18677. <https://doi.org/10.1073/pnas.1110415108> PMID: 22065758
56. Yoshimura S, Gerondopoulos A, Linford A, Rigden DJ, Barr FA. Family-wide characterization of the DENN domain Rab GDP-GTP exchange factors. *J Cell Biol.* 2010; 191:367–381. <https://doi.org/10.1083/jcb.201008051> PMID: 20937701
57. Shen K, Rogala KB, Chou HT, Huang RK, Yu Z, Sabatini DM. Cryo-EM Structure of the Human FLCN-FNIP2-Rag-Ragulator Complex. *Cell.* 2019; 179:1319–1329. <https://doi.org/10.1016/j.cell.2019.10.036> PMID: 31704029
58. Lawrence RE, Fromm SA, Fu Y, Yokom AL, Kim DJ, Thelen AM et al. Structural mechanism of a Rag GTPase activation checkpoint by the lysosomal folliculin complex. *Science.* 2019; 366:971–977. <https://doi.org/10.1126/science.aax0364> PMID: 31672913
59. Baba M, Hong SB, Sharma N, Warren MB, Nickerson ML, Iwamatsu A et al. Folliculin encoded by the BHD gene interacts with a binding protein, FNIP1, and AMPK, and is involved in AMPK and mTOR signaling. *Proc Natl Acad Sci U S A.* 2006; 103:15552–15557. <https://doi.org/10.1073/pnas.0603781103> PMID: 17028174
60. Hasumi H, Baba M, Hong SB, Hasumi Y, Huang Y, Yao M et al. Identification and characterization of a novel folliculin-interacting protein FNIP2. *Gene.* 2008; 415:60–67. <https://doi.org/10.1016/j.gene.2008.02.022> PMID: 18403135
61. Takagi Y, Kobayashi T, Shiono M, Wang L, Piao X, Sun G et al. Interaction of folliculin (Birt-Hogg-Dube gene product) with a novel Fnip1-like (FnipL/Fnlp2) protein. *Oncogene.* 2008; 27:5339–5347. <https://doi.org/10.1038/onc.2008.261> PMID: 18663353
62. Hasumi H, Baba M, Hasumi Y, Lang M, Huang Y, Oh HF et al. Folliculin-interacting proteins Fnip1 and Fnip2 play critical roles in kidney tumor suppression in cooperation with Flcn. *Proc Natl Acad Sci U S A.* 2015; 112:E1624–E1631. <https://doi.org/10.1073/pnas.1419502112> PMID: 25775561
63. Chen J, Futami K, Petillo D, Peng J, Wang P, Knol J et al. Deficiency of FLCN in mouse kidney led to development of polycystic kidneys and renal neoplasia. *PLoS One.* 2008; 3:e3581.

64. Sager RA, Woodford MR, Shapiro O, Mollapour M, Bratslavsky G. Sporadic renal angiomyolipoma in a patient with Birt-Hogg-Dubé: chaperones in pathogenesis. *Oncotarget*. 2018; 9:22220–22229. <https://doi.org/10.18632/oncotarget.25164> PMID: 29774133
65. Nahorski MS, Reiman A, Lim DH, Nookala RK, Seabra L, Lu X et al. Birt Hogg-Dube syndrome-associated FLCN mutations disrupt protein stability *Hum Mutat* 2011; 32:921–929. <https://doi.org/10.1002/humu.21519> PMID: 21538689
66. Matreyek KA, Starita LM, Stephany JJ, Martin B, Chiasson MA, Gray VE et al. Multiplex assessment of protein variant abundance by massively parallel sequencing *Nat Genet* 2018; 50:874–882. <https://doi.org/10.1038/s41588-018-0122-z> PMID: 29785012
67. Roscoe BP, Thayer KM, Zeldovich KB, Fushman D, Bolon DN. Analyses of the effects of all ubiquitin point mutants on yeast growth rate. *J Mol Biol*. 2013; 425:1363–1377.
68. Stein A, Fowler DM, Hartmann-Petersen R, Lindorff-Larsen K. Biophysical and Mechanistic Models for Disease-Causing Protein Variants. *Trends Biochem Sci*. 2019; 44:575–588. <https://doi.org/10.1016/j.tibs.2019.01.003> PMID: 30712981
69. Gonzalez CE, Roberts P, Ostermeier M. Fitness Effects of Single Amino Acid Insertions and Deletions in TEM-1 beta-Lactamase. *J Mol Biol*. 2019; 431:2320–2330. <https://doi.org/10.1016/j.jmb.2019.04.030> PMID: 31034887
70. Arpino JA, Reddington SC, Halliwell LM, Rizkallah PJ, Jones DD. Random single amino acid deletion sampling unveils structural tolerance and the benefits of helical registry shift on GFP folding and structure. *Structure*. 2014; 22:889–898. <https://doi.org/10.1016/j.str.2014.03.014> PMID: 24856363
71. Jones DD. Triplet nucleotide removal at random positions in a target gene: the tolerance of TEM-1 beta-lactamase to an amino acid deletion. *Nucleic Acids Res*. 2005; 33:e80.
72. Banerjee A, Levy Y, Mitra P. Analyzing Change in Protein Stability Associated with Single Point Deletions in a Newly Defined Protein Structure Database. *J Proteome Res*. 2019; 18:1402–1410. <https://doi.org/10.1021/acs.jproteome.9b00048> PMID: 30735617
73. Park H, Bradley P, Greisen P, Jr., Liu Y, Mulligan VK, Kim DE et al. Simultaneous Optimization of Biomolecular Energy Functions on Features from Small Molecules and Macromolecules. *J Chem Theory Comput*. 2016; 12:6201–6212. <https://doi.org/10.1021/acs.jctc.6b00819> PMID: 27766851
74. Alford RF, Leaver-Fay A, Jeliakov JR, O'Meara MJ, DiMaio FP, Park H et al. The Rosetta All-Atom Energy Function for Macromolecular Modeling and Design. *J Chem Theory Comput*. 2017; 13:3031–3048. <https://doi.org/10.1021/acs.jctc.7b00125> PMID: 28430426
75. Jackson EL, Spielman SJ, Wilke CO. Computational prediction of the tolerance to amino-acid deletion in green-fluorescent protein. *PLoS One*. 2017; 12:e0164905. <https://doi.org/10.1371/journal.pone.0164905> PMID: 28369116
76. Mathiassen SG, Larsen IB, Poulsen EG, Madsen CT, Papaleo E, Lindorff-Larsen K et al. A Two-step Protein Quality Control Pathway for a Misfolded DJ-1 Variant in Fission Yeast. *J Biol Chem*. 2015; 290:21141–21153. <https://doi.org/10.1074/jbc.M115.662312> PMID: 26152728
77. Karczewski KJ, Francioli LC, Tiao G, Cummings BB, Alföldi J, Wang Q et al. Variation across 141,456 human exomes and genomes reveals the spectrum of loss-of-function intolerance across human protein-coding genes. *bioRxiv*. 2019;531210:
78. Shiber A, Breuer W, Brandeis M, Ravid T. Ubiquitin conjugation triggers misfolded protein sequestration into quality control foci when Hsp70 chaperone levels are limiting. *Mol Biol Cell*. 2013; 24:2076–2087. <https://doi.org/10.1091/mbc.E13-01-0010> PMID: 23637465
79. Le Goff X, Chesnel F, Delalande O, Couturier A, Dreano S, Le Goff C. et al. Aggregation dynamics and identification of aggregation-prone tumor mutants of the von Hippel-Lindau tumor suppressor protein. *J Cell Sci*. 2016; 129:2638–2650. <https://doi.org/10.1242/jcs.184846> PMID: 27179072
80. Westhoff B, Chapple JP, van der Spuy J, Hohfeld J, Cheetham ME. Hsj1 is a neuronal shuttling factor for the sorting of chaperone clients to the proteasome. *Curr Biol*. 2005; 15:1058–1064. <https://doi.org/10.1016/j.cub.2005.04.058> PMID: 15936278
81. Bartram MP, Mishra T, Reintjes N, Fabretti F, Gharbi H, Adam AC et al. Characterization of a splice-site mutation in the tumor suppressor gene FLCN associated with renal cancer. *BMC Med Genet*. 2017; 18:53. <https://doi.org/10.1186/s12881-017-0416-5> PMID: 28499369
82. Bard JAM, Goodall EA, Greene ER, Jonsson E, Dong KC, Martin A. Structure and Function of the 26S Proteasome. *Annu Rev Biochem*. 2018; 87:697–724. <https://doi.org/10.1146/annurev-biochem-062917-011931> PMID: 29652515
83. Winzeler EA, Shoemaker DD, Astromoff A, Liang H, Anderson K, Andre B et al. Functional characterization of the *S. cerevisiae* genome by gene deletion and parallel analysis. *Science*. 1999; 285:901–906. <https://doi.org/10.1126/science.285.5429.901> PMID: 10436161

84. Kim RQ, Sixma TK. Regulation of USP7: A High Incidence of E3 Complexes. *J Mol Biol.* 2017; 429:3395–3408. <https://doi.org/10.1016/j.jmb.2017.05.028> PMID: 28591556
85. Landrum MJ, Chitipiralla S, Brown GR, Chen C, Gu B, Hart J et al. ClinVar: improvements to accessing data. *Nucleic Acids Res.* 2020; 48:D835–D844. <https://doi.org/10.1093/nar/gkz972> PMID: 31777943
86. Chai Y, Koppenhafer SL, Shoemsmith SJ, Perez MK, Paulson HL. Evidence for proteasome involvement in polyglutamine disease: localization to nuclear inclusions in SCA3/MJD and suppression of polyglutamine aggregation in vitro. *Hum Mol Genet.* 1999; 8:673–682. <https://doi.org/10.1093/hmg/8.4.673> PMID: 10072437
87. Sowa ME, Bennett EJ, Gygi SP, Harper JW. Defining the human deubiquitinating enzyme interaction landscape. *Cell.* 2009; 138:389–403. <https://doi.org/10.1016/j.cell.2009.04.042> PMID: 19615732
88. Maertens GN, El Messaoudi-Aubert S, Elderkin S, Hiom K, Peters G. Ubiquitin-specific proteases 7 and 11 modulate Polycomb regulation of the INK4a tumour suppressor. *EMBO J.* 2010; 29:2553–2565. <https://doi.org/10.1038/emboj.2010.129> PMID: 20601937
89. Hao YH, Fountain MD Jr., Fon TK, Xia F, Bi W, Kang SH et al. USP7 Acts as a Molecular Rheostat to Promote WASH-Dependent Endosomal Protein Recycling and Is Mutated in a Human Neurodevelopmental Disorder. *Mol Cell.* 2015; 59:956–969. <https://doi.org/10.1016/j.molcel.2015.07.033> PMID: 26365382
90. Cummins JM, Rago C, Kohli M, Kinzler KW, Lengauer C, Vogelstein B. Tumour suppression: disruption of HAUSP gene stabilizes p53. *Nature.* 2004; 428:1. <https://doi.org/10.1038/nature02501> PMID: 15058298
91. Li M, Brooks CL, Kon N, Gu W. A dynamic role of HAUSP in the p53-Mdm2 pathway. *Mol Cell.* 2004; 13:879–886. [https://doi.org/10.1016/s1097-2765\(04\)00157-1](https://doi.org/10.1016/s1097-2765(04)00157-1) PMID: 15053880
92. Turnbull AP, Ioannidis S, Krajewski WW, Pinto-Fernandez A, Heride C, Martin ACL et al. Molecular basis of USP7 inhibition by selective small-molecule inhibitors. *Nature.* 2017; 550:481–486. <https://doi.org/10.1038/nature24451> PMID: 29045389
93. Reverdy C, Conrath S, Lopez R, Planquette C, Atmanene C, Collura V et al. Discovery of specific inhibitors of human USP7/HAUSP deubiquitinating enzyme *Chem Biol* 2012; 19:467–477.
94. Samant RS, Livingston CM, Sontag EM, Frydman J. Distinct proteostasis circuits cooperate in nuclear and cytoplasmic protein quality control. *Nature.* 2018; 563:407–411. <https://doi.org/10.1038/s41586-018-0678-x> PMID: 30429547
95. Theodoraki MA, Nillegoda NB, Saini J, Caplan AJ. A network of ubiquitin ligases is important for the dynamics of misfolded protein aggregates in yeast. *J Biol Chem.* 2012; 287:23911–23922. <https://doi.org/10.1074/jbc.M112.341164> PMID: 22593585
96. Gowda NK, Kandasamy G, Froehlich MS, Dohmen RJ, Andreasson C. Hsp70 nucleotide exchange factor Fes1 is essential for ubiquitin-dependent degradation of misfolded cytosolic proteins. *Proc Natl Acad Sci U S A.* 2013; 110:5975–5980. <https://doi.org/10.1073/pnas.1216778110> PMID: 23530227
97. Kandasamy G, Andreasson C. Hsp70-Hsp110 chaperones deliver ubiquitin-dependent and -independent substrates to the 26S proteasome for proteolysis in yeast. *J Cell Sci.* 2018;131. <https://doi.org/10.1242/jcs.210948> PMID: 29507114
98. Connell P, Ballinger CA, Jiang J, Wu Y, Thompson LJ, Hohfeld J et al. The co-chaperone CHIP regulates protein triage decisions mediated by heat-shock proteins. *Nat Cell Biol.* 2001; 3:93–96. <https://doi.org/10.1038/35050618> PMID: 11146632
99. Fang NN, Chan GT, Zhu M, Comyn SA, Persaud A, Deshaies RJ et al. Rsp5/Nedd4 is the main ubiquitin ligase that targets cytosolic misfolded proteins following heat stress. *Nat Cell Biol.* 2014; 16:1227–1237. <https://doi.org/10.1038/ncb3054> PMID: 25344756
100. Yanagitani K, Juszkiwicz S, Hegde RS. UBE2O is a quality control factor for orphans of multiprotein complexes. *Science.* 2017; 357:472–475. <https://doi.org/10.1126/science.aan0178> PMID: 28774922
101. McShane E, Sin C, Zauber H, Wells JN, Donnelly N, Wang X et al. Kinetic Analysis of Protein Stability Reveals Age-Dependent Degradation. *Cell.* 2016; 167:803–815.
102. Nagashima K, Fukushima H, Shimizu K, Yamada A, Hidaka M, Hasumi H et al. Nutrient-induced FNIP degradation by SCFbeta-TRCP regulates FLCN complex localization and promotes renal cancer progression. *Oncotarget.* 2017; 8:9947–9960. <https://doi.org/10.18632/oncotarget.14221> PMID: 28039480
103. Hasumi H, Hasumi Y, Baba M, Nishi H, Furuya M, Vocke CD et al. H255Y and K508R missense mutations in tumour suppressor folliculin (FLCN) promote kidney cell proliferation *Hum Mol Genet.* 2017; 26:354–366.
104. Van GF, Hadida S, Grootenhuys PD, Burton B, Stack JH, Straley KS et al. Correction of the F508del-CFTR protein processing defect in vitro by the investigational drug VX-809 *Proc Natl Acad Sci U S A.* 2011; 108:18843–18848. <https://doi.org/10.1073/pnas.1105787108> PMID: 21976485

105. Yang C, Huntoon K, Ksendzovsky A, Zhuang Z, Lonser RR. Proteostasis modulators prolong mis-sense VHL protein activity and halt tumor progression. *Cell Rep*. 2013; 3:52–59.
106. Joerger AC, Fersht AR. The p53 Pathway: Origins, Inactivation in Cancer, and Emerging Therapeutic Approaches. *Annu Rev Biochem*. 2016; 85:375–404. <https://doi.org/10.1146/annurev-biochem-060815-014710> PMID: 27145840
107. Kampmeyer C, Nielsen SV, Clausen L, Stein A, Gerdes AM, Lindorff-Larsen K et al. Blocking protein quality control to counter hereditary cancers. *Genes Chromosomes Cancer*. 2017; 56:823–831. <https://doi.org/10.1002/gcc.22487> PMID: 28779490
108. Gietz RD, Woods RA. Transformation of yeast by lithium acetate/single-stranded carrier DNA/polyethylene glycol method *Methods Enzymol*. 2002; 350:87–96. [https://doi.org/10.1016/s0076-6879\(02\)50957-5](https://doi.org/10.1016/s0076-6879(02)50957-5) PMID: 12073338
109. Cox JS, Chapman RE, Walter P. The unfolded protein response coordinates the production of endoplasmic reticulum protein and endoplasmic reticulum membrane *Mol Biol Cell*. 1997; 8:1805–1814. <https://doi.org/10.1091/mbc.8.9.1805> PMID: 9307975
110. Tong AH, Boone C. High-Throughput Strain Construction and Systematic Synthetic Lethal Screening in *Saccharomyces cerevisiae*. *Methods in Microbiology*. 2007; 36:369–386.
111. Webb B, Sali A. Comparative Protein Structure Modeling Using MODELLER *Curr Protoc Protein Sci*. 2016; 86:2.